

# Two-dimensional charge distributions of the $\Delta$ baryon: Interpolation between the nonrelativistic and ultrarelativistic limit

Ki-Hoon Hong,<sup>1,\*</sup> June-Young Kim,<sup>2,†</sup> and Hyun-Chul Kim<sup>1,3,‡</sup>

<sup>1</sup>*Department of Physics, Inha University, Incheon 22212, Republic of Korea*

<sup>2</sup>*Theory Center, Jefferson Lab, Newport News, VA 23606, USA*

<sup>3</sup>*School of Physics, Korea Institute for Advanced Study (KIAS), Seoul 02455, Republic of Korea*

(Dated: January 24, 2023)

We investigate how the charge distributions of both the unpolarized and transversely polarized  $\Delta$  baryon change as the longitudinal momentum ( $P_z$ ) of the  $\Delta$  baryon increases from  $P_z = 0$  to  $P_z = \infty$  in a Wigner phase-space perspective. When the  $\Delta$  baryon is longitudinally polarized, its two-dimensional charge distribution is kept to be spherically symmetric with  $P_z$  varied, whereas when the  $\Delta$  baryon is transversely polarized along the  $x$ -axis, the quadrupole contribution emerges at the rest frame ( $P_z = 0$ ). When  $P_z$  grows, the electric dipole and octupole moments are induced. The induced dipole moment dominates over other higher multipole contributions and governs the deformation of the charge distribution of the  $\Delta$  baryon.

## I. INTRODUCTION

The electromagnetic (EM) form factors of the nucleon have been one of the essential observables in understanding its structure well over decades. They provide crucial information on the charge and magnetization distributions inside a nucleon. This interpretation assumes that the nucleon is at rest in the Breit frame (BF) [1]. This assumption is valid only if the nucleon's spatial size  $R_N$  were larger than the Compton wavelength  $1/M_N$ , so the spatial wave functions could have been well defined. In reality, however, the size of the nucleon is comparable to  $1/M_N$ , so the nucleon wave function is no more localized below the Compton wavelength. It causes ambiguous relativistic corrections that mar the probabilistic interpretation of the 3D EM distributions in the BF [2–4]. This flaw of the 3D charge and magnetization distributions was already pointed out in the 1950s [5]. To understand the EM distributions of the nucleon without any ambiguity, one needs to view the nucleon from the light-front (LF) or, equivalently, the infinite momentum frame (IMF), where the relativistic corrections are kinematically suppressed. Then, the charge distribution emerges in the two-dimensional (2D) plane transverse to the nucleon momentum with the probabilistic meaning properly borne [2, 3]. It is obtained as the 2D Fourier transform of the EM form factors and called the transverse charge distribution of the nucleon [6, 7]. The only problem with the transverse charge distribution is that we lose information along the infinite momentum direction. Since then, the transverse charge distributions of the nucleon,  $\Delta$  baryon, deuteron, pion, kaon, and  $\rho$  meson have been extensively studied [8–33] (see also a review [34]).

When the transverse charge density of the neutron was reported [6], many were perplexed by the result: While the positive charge is centered in the 3D charge distribution of the neutron, the negative one was situated in the center of the neutron for the neutron 2D transverse charge density. Recently, Lorcé resolved the discrepancy by showing that when the longitudinal momentum increases from the rest to infinity, the charge distribution in the transverse plane undergoes drastic changes from the positive center value to the negative one [35]. As the longitudinal momentum grows, a Wigner rotation and a mixing of the four-current components under Lorentz boost give rise to a magnetization contribution [35–37], which makes the sign of the neutron transverse charge density is changed to be negative. In doing so, Lorcé introduced the elastic frame (EF) to interpolate from the BF to the IMF in the Wigner phase-space perspective, which makes it possible to observe the change in the charge distribution explicitly as the longitudinal momentum increases. This approach was extended to the case of the polarized nucleon [38], where the Abel tomography was emphasized. It was recently elaborated and enlarged by considering the EM distributions for the spin-0 and spin-1/2 particles [39] and the EM and energy-momentum tensor (EMT) distributions of the spin-1 particle [25]. Compared to the spin-0 and -1/2 particles [35, 39, 40], the spin-1 particle reveals rather complicated multipole structures [22, 25, 40]. In this work, we want to investigate the multipole structure of the EM distributions for the spin-3/2  $\Delta$  baryon and see how they are altered under Lorentz boost.

The EM form factors of the  $\Delta$  baryon can be parametrized in terms of four multipole form factors [41] (see also a review [42]): electric monopole (E0), quadrupole (E2), magnetic dipole (M1), and octupole (M3) ones. While it

\* E-mail: kihoon@inha.edu

† E-mail: jykim@jlab.org

‡ E-mail: hchkim@inha.ac.kr

is extremely difficult to measure them experimentally because of the  $\Delta$ 's ephemeral nature, the  $\Delta$  EM form factors and corresponding transverse charge densities were computed in lattice QCD [19, 41]. In the rest BF, we can define four frame-dependent functions, which are respectively related to the EM multipole form factors. The Lorentz boost induces the electric dipole (E1) and octupole (E3) contributions to the transverse charge densities of the  $\Delta$  baryon. In the IMF, all the frame-dependent functions coming from the third spatial component of the EM four current become equivalent to those from the temporal one. It is crucial to analyze these consequences arising from the Lorentz boost. In this work, thus, we examine the expressions for the  $\Delta$  baryon matrix elements of the EM current in terms of the frame-dependent functions defined in the 2D EF. They are given as the functions of the momentum transfer  $t$  and the longitudinal momentum  $P_z$ . For any values of  $P_z$ , we are able to define the frame-dependent functions and their 2D Fourier transforms, so each contribution to the transverse  $\Delta$  charge densities can be examined with the  $P_z$  given. If we take  $P_z = 0$ , the frame-dependent functions are reduced to the EM multipole form factors. To investigate the transverse charge densities of the moving  $\Delta$  baryon, we need information on the EM form factors. In the present work, we will take the numerical results of the EM form factors obtained in the SU(3) chiral quark-soliton model [43]. We will then visualize in the 2D space how the charge distributions are deformed under the Lorentz boost.

The present work is organized as follows: In Section II, we construct the formalism for the multipole structure of the transverse charge densities of the  $\Delta$  baryon. In Section III, we present the numerical results for the transverse charge distributions interpolating from the BF to the IMF. We also examine each contribution of the multipole components to the transverse charge distributions of the moving  $\Delta^+$  and  $\Delta^0$  and discuss it. In Section IV, we summarize and draw conclusions of the current work. In Appendix, we list the explicit expressions for the frame-dependent functions.

## II. MULTIPOLE STRUCTURE OF THE TRANSVERSE CHARGE DENSITIES

The matrix element of the EM current is defined as

$$J^\mu(x) = \bar{\psi}(x)\gamma^\mu\hat{Q}\psi(x), \quad (1)$$

where  $\psi(x)$  denotes the quark field. The charge operator of the quarks  $\hat{Q}$  is written in terms of the flavor SU(3) Gell-Mann matrices  $\lambda_3$  and  $\lambda_8$

$$\hat{Q} = \begin{pmatrix} \frac{2}{3} & 0 & 0 \\ 0 & -\frac{1}{3} & 0 \\ 0 & 0 & -\frac{1}{3} \end{pmatrix} = \frac{1}{2} \left( \lambda_3 + \frac{1}{\sqrt{3}}\lambda_8 \right). \quad (2)$$

The matrix elements of the EM current between the  $\Delta$  baryon states with spin 3/2 can be parametrized in terms of four form factors  $F_i^*$  ( $i = 1, \dots, 4$ ) as follows:

$$\begin{aligned} \langle \Delta(p', \sigma') | eJ^\mu(0) | \Delta(p, \sigma) \rangle = & -e_B \bar{u}^\alpha(p', \sigma') \left[ \gamma^\mu \left\{ F_1^*(t)g_{\alpha\beta} + F_3^*(t)\frac{q_\alpha q_\beta}{4M_\Delta^2} \right\} \right. \\ & \left. + i\frac{\sigma^{\mu\nu}q_\nu}{2M_\Delta} \left\{ F_2^*(t)g_{\alpha\beta} + F_4^*(t)\frac{q_\alpha q_\beta}{4M_\Delta^2} \right\} \right] u^\beta(p, \sigma), \end{aligned} \quad (3)$$

where  $M_\Delta$  denotes the mass of the  $\Delta$  baryon, and  $e_B$  stands for the corresponding electric charge in unit of  $e$ .  $q$  designates the momentum transfer  $q = p' - p$  and its square is given as  $q^2 = t$  with  $-t > 0$ .  $u^\alpha(p, \sigma)$  represents the Rarita-Schwinger spinor, carrying the momentum  $p$  and the spin component  $\sigma$  projected along the direction of the momentum. The explicit expression for the Rarita-Schwinger spinor is given by

$$u^\mu(p, \sigma) = \sum_{\lambda, s} C_{1\lambda\frac{1}{2}s}^{\frac{3}{2}\sigma} u_s(p) \epsilon_\lambda^\mu(p), \quad \text{and} \quad u_s(p) = \sqrt{M_\Delta + p_0} \left( \frac{1}{M_\Delta + p_0} \right) \phi_s, \quad (4)$$

where  $u_s(p)$  and  $\phi_s$  stand for the Dirac and Pauli spinors with its spin polarization  $s$ , respectively. Here, we choose the canonical spin states (see relevant discussions [35, 44, 45]). By coupling the Dirac spinor to the spin-one polarization vector, one can construct the Rarita-Schwinger spinor. The spin-one vector  $\epsilon^\mu$  in any frame is expressed by

$$\epsilon_\lambda^\mu(p) = \left( \frac{\hat{e}_\lambda \cdot \vec{p}}{M_\Delta}, \hat{e}_\lambda + \frac{\vec{p}(\hat{e}_\lambda \cdot \vec{p})}{M_\Delta(M_\Delta + P_0)} \right), \quad (5)$$

where  $\hat{e}$  is the polarization vector in the rest frame.

$$\hat{e}_{+1} = \frac{1}{\sqrt{2}}(-1, -i, 0), \quad \hat{e}_0 = (0, 0, 1), \quad \hat{e}_{-1} = \frac{1}{\sqrt{2}}(1, -i, 0). \quad (6)$$

In order to discuss the multipole structure of the EM form factors in a systematical way, it is convenient to introduce the rank- $n$  irreducible tensors and multipole operators in 2D space. The rank- $n$  irreducible tensors in coordinate (or momentum) space are defined by

$$X_0 := 1, \quad X_n^{i_1 \dots i_n} := \frac{(-1)^{n+1}}{(2n-2)!!} x_\perp^n \partial^{i_1} \dots \partial^{i_n} \ln x_\perp \quad \text{with } n > 0, i_n = 1, 2. \quad (7)$$

For a spin-3/2 baryon, the quadrupole- and octupole-spin operators  $\hat{Q}^{ij}$  (rank-2 tensor) and  $\hat{O}^{ijk}$  (rank-3 tensor) appear in the matrix element of the EM current and are respectively defined in terms of the spin operator  $\hat{S}^i$  as follows:

$$\begin{aligned} \hat{Q}^{ij} &:= \frac{1}{2} \left[ \hat{S}^i \hat{S}^j + \hat{S}^j \hat{S}^i - \frac{2}{3} S(S+1) \delta^{ij} \right], \\ \hat{O}^{ijk} &:= \frac{1}{6} \left[ \hat{S}^i \hat{S}^j \hat{S}^k + \hat{S}^j \hat{S}^i \hat{S}^k + \hat{S}^k \hat{S}^j \hat{S}^i + \hat{S}^j \hat{S}^k \hat{S}^i + \hat{S}^i \hat{S}^k \hat{S}^j + \hat{S}^k \hat{S}^i \hat{S}^j \right. \\ &\quad \left. - \frac{6S(S+1)-2}{5} (\delta^{ij} \hat{S}^k + \delta^{ik} \hat{S}^j + \delta^{kj} \hat{S}^i) \right]. \end{aligned} \quad (8)$$

Since the tensor operators are irreducible, so they are fully symmetrized under the exchanges of the indices  $i, j, k = 1, 2, 3$  and traceless ( $\hat{Q}^{ii} = 0$  and  $\delta_{ij} \hat{O}^{ijk} = 0$ ). The spin operators can be expressed in terms of SU(2) Clebsch-Gordan coefficients in the spherical basis

$$\hat{S}_{\sigma'\sigma}^a = \sqrt{S(S+1)} C_{S\sigma 1a}^{S\sigma'} \quad \text{with } (a = 0, \pm 1, \sigma, \sigma' = 0, \dots, \pm S). \quad (9)$$

To see how the matrix element of the EM current is changed under Lorentz boost, we need to employ the EF, where space-like momentum transfer  $\mathbf{q}$  lies in the transverse plane with conditions  $q^0 = 0$  and  $\mathbf{P} \neq 0$ , as suggested in Ref. [35]. Without loss of generality, in the EF, the average momentum  $P = (p' + p)/2$  and momentum transfer  $q$  with the on-shell constraint are taken to be

$$P = (P_0, \vec{0}, P_z) \quad q = (0, \vec{q}_\perp, 0), \quad P_0 = \sqrt{(1+\tau)M_\Delta^2 + P_z^2}, \quad (10)$$

with  $\tau = -t/(4M_\Delta^2)$ . Then, the matrix element of the temporal component of the EM current  $J^0$  in the EF from Eq. (3) is written in terms of the multipole  $n$ -rank irreducible tensors in momentum space and in spin polarization together with the frame-dependent scalar functions  $G_{E0, E1, E2, E3}$ :

$$\begin{aligned} \frac{\langle J^0 \rangle_{\sigma'\sigma}}{2P^0} &= \left\{ G_{E0}(t; P_z) - \frac{2}{3} \tau G_{E2}(t; P_z) \right\} \delta_{\sigma'\sigma} + \left\{ G_{E0}^{a'a}(t; P_z) + \frac{4}{3} \tau G_{E2}(t; P_z) \right\} \delta_{a'a} \\ &\quad + 2\sqrt{\tau} \left\{ G_{E1}(t; P_z) - \frac{2}{5} \tau G_{E3}(t; P_z) \right\} i\epsilon^{ij3} S_{\sigma'\sigma}^i X_1^j(\theta_{q_\perp}) \\ &\quad + 2\sqrt{\tau} \left\{ G_{E1}^{a'a}(t; P_z) + \tau G_{E3}(t; P_z) \right\} i\epsilon^{ij3} S_{a'a}^i X_1^j(\theta_{q_\perp}) \\ &\quad + \frac{4}{3} \tau G_{E2}(t; P_z) Q_{\sigma'\sigma}^{ij} X_2^{ij}(\theta_{q_\perp}) + 8\tau^{3/2} G_{E3}(t; P_z) i\epsilon^{3jk} O_{\sigma'\sigma}^{jml} X_3^{klm}(\theta_{q_\perp}), \end{aligned} \quad (11)$$

where we introduce the following short-handed notation  $\delta_{a'a} = \delta_{\sigma'a'} \delta_{\sigma a} \delta_{\sigma'\sigma}$  with  $a', a = -\frac{1}{2}, \frac{1}{2}$  and  $\langle J^\mu \rangle_{\sigma'\sigma} := \langle \Delta(p', \sigma') | \hat{J}^\mu(0) | \Delta(p, \sigma) \rangle$ . Here,  $\theta_{q_\perp}$  denotes the 2D angle of the  $q_\perp$  variable.

Before discussing the EM form factor in the 2D EF, we want briefly to mention the 2D and 3D BFs. To study the 3D spatial distributions, the 3D BF is adopted, where  $q^0 = 0$  and  $\mathbf{P} = 0$ . It yields the well-known Sach-type or multipole form factors. Since we interpolate the 2D BF to 2D IMF distributions in this work, we introduce the 2D BF, where each component of the four momenta  $P$  and  $q$  are taken to be the same as in the 3D BF. It can simply be achieved by taking  $q_z = 0$ .

In the 3D BF,  $\langle J^0 \rangle_{\sigma'\sigma}$  yields normally two contributions: the electric monopole ( $E0$ ) and electric quadrupole ( $E2$ ) ones. However, the projection from the 3D BF to the 2D one and the Lorentz boost induce various contributions. Firstly, in the presence of the  $E2$  contribution, the projection from the 3D BF to the 2D one induces the monopole contribution. In addition, it is split into the spin-polarizations  $\sigma = -\frac{3}{2}, \dots, \frac{2}{3}$  and its subsystem  $a = -\frac{1}{2}, \frac{1}{2}$ . Secondly, under the Lorentz boost, the matrix element of the temporal component of the EM current  $J^0$  is subject to the Wigner spin rotation and the admixture with the spatial component of the EM current. It results in the induced electric dipole ( $E1$ ) and induces the  $E3$  contributions, and the Lorentz boost brings about the frame dependence on  $P_z$  in

the matrix element of  $J^0$ . These effects from the Lorentz boost are conveyed to the frame-dependent  $G_{E0,E1,E2,E3}$  given as the functions of  $P_z$  and  $t$ . The explicit expressions for them are listed in Appendix A. In the BF ( $P_z = 0$ ), these frame-dependent functions are reduced to the 2D BF expressions:

$$\frac{\langle J^0 \rangle_{\sigma'\sigma}}{2P^0} \stackrel{P_z \rightarrow 0}{=} \frac{1}{\sqrt{1+\tau}} \left[ \left( G_{E0}(t) + \frac{1}{3}\tau G_{E2}(t) \right) \delta_{\sigma'\sigma} - \frac{2\tau}{3} G_{E2}(t) \delta_{a'a} - \frac{2\tau}{3} G_{E2}(t) Q_{\sigma'\sigma}^{ij} X_2^{ij}(\theta_{\Delta\perp}) \right]. \quad (12)$$

In the 2D BF limit, we recover the traditional definitions of the Sach-type EM form factors together with the relativistic factor  $1/\sqrt{1+\tau}$ , which comes into play when interpolating the BF expressions to the IMF ones:

$$\begin{aligned} G_{E0}(t; P_z = 0) &= \frac{1}{\sqrt{1+\tau}} G_{E0}(t), & G_{E0}^{a'a}(t; P_z = 0) &= 0, & G_{E1}(t; P_z = 0) &= 0, \\ G_{E1}^{a'a}(t; P_z = 0) &= 0, & G_{E2}(t; P_z = 0) &= -\frac{1}{2\sqrt{1+\tau}} G_{E2}(t), & G_{E3}(t; P_z = 0) &= 0, \end{aligned} \quad (13)$$

where the EM multipole form factors are expressed in terms of  $F_i^*$ :

$$\begin{aligned} G_{E0}(t) &= \left( 1 + \frac{2}{3}\tau \right) \left[ F_1^*(t) - \tau F_2^*(t) \right] - \frac{1}{3}\tau(1+\tau) \left[ F_3^*(t) - \tau F_4^*(t) \right], \\ G_{E2}(t) &= \left[ F_1^*(t) - \tau F_2^*(t) \right] - \frac{1}{2}(1+\tau) \left[ F_3^*(t) - \tau F_4^*(t) \right], \\ G_{M1}(t) &= \left( 1 + \frac{4}{5}\tau \right) \left[ F_1^*(t) + F_2^*(t) \right] - \frac{2}{5}\tau(1+\tau) \left[ F_3^*(t) + F_4^*(t) \right], \\ G_{M3}(t) &= \left[ F_1^*(t) + F_2^*(t) \right] - \frac{1}{2}(1+\tau) \left[ F_3^*(t) + F_4^*(t) \right]. \end{aligned} \quad (14)$$

They are called, respectively, the electric monopole ( $E0$ ), electric quadrupole ( $E2$ ), magnetic dipole ( $M1$ ), and magnetic octupole ( $M3$ ) form factors. The  $M1$  and  $M3$  form factors will be obtained in the matrix element of the spatial component of the EM current  $J^i$ . By taking  $P_z \rightarrow \infty$  in Eq.(11), we can naturally recover the results from the LF formalism [19]:

$$\begin{aligned} G_{E0}(t; P_z \rightarrow \infty) &= \frac{1}{1+\tau} \left( G_{E0}(t) + \frac{1}{3}\tau G_{M1}(t) - \frac{4}{15}\tau^2 G_{M3}(t) \right), \\ G_{E0}^{a'a}(t; P_z \rightarrow \infty) &= -\frac{4\tau}{(1+\tau)^2} \left[ G_{E0}(t) + \frac{1}{3}\tau G_{E2}(t) - \frac{1}{3}(2-\tau) G_{M1}(t) - \frac{\tau}{15}(2-\tau) G_{M3}(t) \right], \\ G_{E1}(t; P_z \rightarrow \infty) &= -\frac{1}{(1+\tau)^2} \left[ \left( 1 + \frac{\tau}{15} \right) G_{E0}(t) + \frac{2\tau}{15} \left( 2 - \frac{\tau}{3} \right) G_{E2}(t) - \frac{1}{3} \left( 1 - \frac{9}{5}\tau \right) G_{M1}(t) + \frac{14}{75}\tau^2 G_{M3}(t) \right], \\ G_{E1}^{a'a}(t; P_z \rightarrow \infty) &= \frac{2\tau}{3(1+\tau)^2} \left[ G_{E0}(t) - G_{M1}(t) + \frac{\tau}{3} G_{E2}(t) - \frac{\tau}{5} G_{M3}(t) \right], \\ G_{E2}(t; P_z \rightarrow \infty) &= \frac{1}{2(1+\tau)^2} \left[ 3G_{E0}(t) - G_{E2}(t) - (2-\tau) G_{M1}(t) - \frac{\tau}{5} (7+4\tau) G_{M3}(t) \right], \\ G_{E3}(t; P_z \rightarrow \infty) &= -\frac{1}{6(1+\tau)^2} \left[ G_{E0}(t) - G_{E2}(t) \left( 1 + \frac{2\tau}{3} \right) - G_{M1}(t) + \left( 1 + \frac{4\tau}{5} \right) G_{M3}(t) \right]. \end{aligned} \quad (15)$$

At the zero momentum transfer  $t = 0$  in Eq.(15), we have

$$\begin{aligned} G_{E0}(t; P_z \rightarrow \infty) &= G_{E0}(0), & G_{E0}^{a'a}(t; P_z \rightarrow \infty) &= 0, & G_{E1}(t; P_z \rightarrow \infty) &= -\left[ G_{E0}(0) - \frac{1}{3} G_{M1}(0) \right], \\ G_{E1}^{a'a}(t; P_z \rightarrow \infty) &= 0, & G_{E2}(t; P_z \rightarrow \infty) &= \frac{1}{2} \left[ 3G_{E0}(0) - G_{E2}(0) - 2G_{M1}(0) \right], \\ G_{E3}(t; P_z \rightarrow \infty) &= -\frac{1}{6} \left[ G_{E0}(0) - G_{E2}(0) - G_{M1}(0) + G_{M3}(0) \right]. \end{aligned} \quad (16)$$

The above results are consistent with those in Ref. [19]. It is also interesting to study how the spatial components of the EM current varies under the Lorentz boost. Since we take the  $z$ -axis as a boost direction,  $J^3$  and  $J_\perp^i$  with  $i = 1, 2$

will behave differently under the Lorentz boost. In the 2D EF, the matrix element of the transverse component of the EM current  $J_{\perp}^i$  is given by

$$\begin{aligned} \frac{\langle J_{\perp}^i \rangle_{\sigma'\sigma}}{2P_0} &= 2\sqrt{\tau} \left[ G_{M1}^{\perp}(t; P_z) - \frac{1}{5}\tau G_{M3}^{\perp}(t; P_z) \right] i\epsilon^{i3k} S_{\sigma'\sigma}^3 X_1^k(\theta_{\Delta_{\perp}}) \\ &+ 2\sqrt{\tau} \left[ G_{M1}^{\perp, a'a}(t; P_z) + 2\tau G_{M3}^{\perp}(t; P_z) \right] i\epsilon^{i3k} S_{a'a}^3 X_1^k(\theta_{\Delta_{\perp}}) + 4\tau G_{M2}^{\perp}(t; P_z) Q_{\sigma'\sigma}^{l3} X_2^{li}(\theta_{\Delta_{\perp}}) \\ &- 2\tau G_{M2}^{\perp}(t; P_z) Q_{\sigma'\sigma}^{i3} + 4\tau\sqrt{\tau} G_{M3}^{\perp}(t; P_z) i\epsilon^{i3k} (2O_{\sigma'\sigma}^{3ml} X_3^{klm}(\theta_{\Delta_{\perp}}) + O_{\sigma'\sigma}^{3kl} X_1^l(\theta_{\Delta_{\perp}})). \end{aligned} \quad (17)$$

The frame-dependent functions from the transverse components of the EM current are labeled by  $\perp$  in the superscript. The matrix element of the transverse EM current yields the magnetic dipole and octupole contributions together with the induced magnetic quadrupole one. In the 2D BF limit, the frame-dependent functions  $G_{M1}^{\perp}, G_{M1}^{a'a, \perp}, G_{M2}^{\perp}, G_{M3}^{\perp}$  are reduced to the Sach-type magnetic dipole (M1) and magnetic octupole (M1) form factors given in Eq. (14):

$$\begin{aligned} \frac{\langle J_{\perp}^i \rangle_{\sigma'\sigma}}{2P_0} \xrightarrow{P_z \rightarrow 0} & \frac{2}{3} \sqrt{\frac{\tau}{1+\tau}} \left( G_{M1}(t) - \frac{\tau}{10} G_{M3}(t) \right) i\epsilon^{i3k} S_{\sigma'\sigma}^3 X_1^k(\theta_{\Delta_{\perp}}) - \frac{2}{3} \tau \sqrt{\frac{\tau}{1+\tau}} G_{M3}(t) i\epsilon^{i3k} S_{a'a}^3 X_1^k(\theta_{\Delta_{\perp}}) \\ & - \frac{2}{3} \tau \sqrt{\frac{\tau}{1+\tau}} G_{M3}(t) i\epsilon^{i3k} \left( 2O_{\sigma'\sigma}^{3ml} X_3^{klm}(\theta_{\Delta_{\perp}}) + O_{\sigma'\sigma}^{3kl} X_1^l(\theta_{\Delta_{\perp}}) \right), \end{aligned} \quad (18)$$

where

$$\begin{aligned} G_{M1}^{\perp}(t; P_z = 0) &= \frac{1}{3\sqrt{1+\tau}} G_{M1}(t), \quad G_{M1}^{\perp, a'a}(t; P_z = 0) = 0, \\ G_{M2}^{\perp}(t; P_z = 0) &= 0, \quad G_{M3}^{\perp}(t; P_z = 0) = -\frac{1}{6\sqrt{1+\tau}} G_{M3}(t). \end{aligned} \quad (19)$$

Note that the induced magnetic dipole contribution  $G_{M2}^{\perp}$  vanishes. Thus, we can regain the results from the LF formalism [19] as in the electric case. We observe that the unusual structure  $O^{3kl} X_1^l$  in the last term in Eq. (18) is induced by the projection from the 3D space to 2D one. As shown in the case of the nucleon [39], all the relevant frame-dependent functions go to zero in the IMF due to the  $P_z$  suppression:

$$G_{M1}^{\perp}(t; P_z \rightarrow \infty) = 0, \quad G_{M1}^{\perp, a'a}(t; P_z \rightarrow \infty) = 0, \quad G_{M2}^{\perp}(t; P_z \rightarrow \infty) = 0, \quad G_{M3}^{\perp}(t; P_z \rightarrow \infty) = 0, \quad (20)$$

so that the matrix element of the transverse components of the EM current  $J_{\perp}^i$  becomes zero in the IMF, i.e.,  $\frac{\langle J_{\perp}^i \rangle}{2P_0} \xrightarrow{P_z \rightarrow \infty} 0$ . Lastly, we obtained the expression of the matrix element of the  $z$ -component of the EM current as follows

$$\begin{aligned} \frac{\langle J^3 \rangle_{\sigma'\sigma}}{2P_0} &= \left[ G_{M0}^3(t; P_z) - \frac{2}{3}\tau G_{M2}^3 - 4\tau G_{M2}^{\perp} \right] \delta_{\sigma'\sigma} + \left[ G_{M0}^{3, a'a}(t; P_z) + \frac{4}{3}\tau G_{M2}^3(t; P_z) + 8\tau G_{M2}^{\perp}(t; P_z) \right] \delta_{a'a} \\ &+ 2\sqrt{\tau} \left[ G_{M1}^3 - \frac{2}{5}\tau G_{M3}^3 \right] i\epsilon^{3jk} S_{\sigma'\sigma}^j X_1^k(\theta_{\Delta_{\perp}}) + 2\sqrt{\tau} \left[ G_{M1}^{3, a'a} + \tau G_{M3}^3 \right] i\epsilon^{3jk} S_{a'a}^j X_1^k(\theta_{\Delta_{\perp}}) \\ &+ \frac{4}{3}\tau G_{M2}^3 Q_{\sigma'\sigma}^{lm} X_2^{lm}(\theta_{\Delta_{\perp}}) + 8\tau\sqrt{\tau} G_{M3}^3 i\epsilon^{3jk} O_{\sigma'\sigma}^{jml} X_3^{klm}(\theta_{\Delta_{\perp}}). \end{aligned} \quad (21)$$

The frame-dependent functions from the  $z$ -component of the EM current are labeled by the 3 in the superscript. The  $J^3$  matrix element produces the M1 and M3 contributions together with the induced M0 and M2 contributions. Similar to the transverse component of the EM current  $J_{\perp}^i$ , the  $z$ -component of the EM current is reduced to the Sach-type magnetic dipole and octupole form factors at  $P_z = 0$ , and the other frame-dependent functions vanish:

$$\begin{aligned} \frac{\langle J^3 \rangle_{\sigma'\sigma}}{2P_0} \xrightarrow{P_z \rightarrow 0} & \frac{2}{3} \sqrt{\frac{\tau}{1+\tau}} \left( G_{M1} + \frac{\tau}{5} G_{M3} \right) i\epsilon^{3jk} S_{\sigma'\sigma}^j X_1^k - \frac{1}{3} \tau \sqrt{\frac{\tau}{1+\tau}} G_{M3} i\epsilon^{3jk} S_{a'a}^j X_1^k \\ & - \frac{4}{3} \tau \sqrt{\frac{\tau}{1+\tau}} G_{M3} i\epsilon^{3jk} O_{\sigma'\sigma}^{jml} X_3^{klm}, \end{aligned} \quad (22)$$

where

$$\begin{aligned} G_{M0}^3(t; P_z = 0) &= 0, \quad G_{M1}^3(t; P_z = 0) = \frac{1}{3\sqrt{1+\tau}} G_{M1}, \quad G_{M1}^{3, a'a}(t; P_z = 0) = 0, \\ G_{M0}^{3, a'a}(t; P_z = 0) &= 0, \quad G_{M2}^3(t; P_z = 0) = 0, \quad G_{M3}^3(t; P_z = 0) = -\frac{1}{6\sqrt{1+\tau}} G_{M3}. \end{aligned} \quad (23)$$

In the IMF, all the frame-dependent functions of the  $J^3$  turn out to be equivalent to those of the  $J^0$ :

$$\begin{aligned} G_{M0}^3(t; P_z \rightarrow \infty) &= G_{E0}(t; P_z \rightarrow \infty), & G_{M0}^{3,a'a}(t; P_z \rightarrow \infty) &= G_{E0}^{a'a}(t; P_z \rightarrow \infty), \\ G_{M1}^3(t; P_z \rightarrow \infty) &= G_{E1}(t; P_z \rightarrow \infty), & G_{M1}^{3,a'a}(t; P_z \rightarrow \infty) &= G_{E1}^{a'a}(t; P_z \rightarrow \infty), \\ G_{M2}^3(t; P_z \rightarrow \infty) &= G_{E2}(t; P_z \rightarrow \infty), & G_{M3}^3(t; P_z \rightarrow \infty) &= G_{E3}(t; P_z \rightarrow \infty), \end{aligned} \quad (24)$$

so we have  $\frac{\langle J^3 \rangle}{2P_0} \xrightarrow{P_z \rightarrow \infty} \frac{\langle J^0 \rangle}{2P_0}$ . A similar relation for the nucleon was first derived in Ref. [39], and we see that such a relation is also satisfied for the  $\Delta$  baryon as shown in the current work.

We are now in a position to define the transverse charge distributions. In this work, we will consider the temporal component of the EM current only, i.e.,  $J^0$ . In the BF, the 3D distribution is traditionally defined as a 3D Fourier transformation of the corresponding form factor. As mentioned in the Introduction, the baryon cannot be localized below the Compton wavelength, which causes ambiguous relativistic corrections. Recently, these 3D distributions in the BF and the 2D distributions of the moving baryon in the EF were understood as quasi-probabilistic distributions in the phase space or the Wigner distributions [25, 35, 46, 47]. We will first construct the transverse charge distribution of the moving  $\Delta$  baryon by introducing the EF and will show the connection between the 2D BF and 2D IMF distributions.

In the Wigner phase-space perspective, the Fourier transform of the matrix element of the EM current conveys information on the internal structure of the particle. Since the average momentum and momentum transfer of the initial and final states are respectively given by  $P = (P_0, \mathbf{0}_\perp, P_z)$  and  $q = (0, \mathbf{q}_\perp, 0)$  in EF, the EF distributions depend on the impact parameter  $\mathbf{x}_\perp$  and momentum  $\mathbf{P} = (\mathbf{0}, P_z)$ , where the  $\Delta$  baryon moves along the  $z$ -direction without loss of generality. Thus, the charge distribution can be expressed as the 2D Fourier transform of the matrix element  $\langle \Delta(p', \sigma') | J^\mu(0) | \Delta(p, \sigma) \rangle$ :

$$\begin{aligned} \rho_{\text{ch}}(\mathbf{x}_\perp, \sigma', \sigma; P_z) &= \int \frac{d^2 q_\perp}{(2\pi)^2} \frac{\langle J^0 \rangle_{\sigma'\sigma}}{2P^0} e^{-i\vec{q}_\perp \cdot \vec{x}_\perp} \\ &= \rho_0(x_\perp; P_z) \delta_{\sigma'\sigma} + \rho_0^{a'a}(x_\perp; P_z) \delta_{a'a} \\ &\quad + \rho_1(x_\perp; P_z) \epsilon^{ij3} X_1^j(\theta_{x_\perp}) S_{\sigma'\sigma}^i + \rho_1^{a'a}(x_\perp; P_z) \epsilon^{ij3} X_1^j(\theta_{x_\perp}) S_{a'a}^i \\ &\quad + \rho_2(x_\perp; P_z) Q_{\sigma'\sigma}^{ij} X_2^{ij}(\theta_{x_\perp}) + \rho_3(x_\perp; P_z) \epsilon^{3jk} O_{\sigma'\sigma}^{jml} X^{klm}(\theta_{x_\perp}), \end{aligned} \quad (25)$$

where

$$\begin{aligned} \rho_0(x_\perp; P_z) &= \tilde{G}_0(x_\perp; P_z), \quad \rho_0^{a'a} = \tilde{G}_0^{a'a}(x_\perp; P_z), \quad \rho_1(x_\perp; P_z) = -\frac{1}{M_\Delta} \frac{d}{dx_\perp} \tilde{G}_1(x_\perp; P_z), \\ \rho_1^{a'a}(x_\perp; P_z) &= -\frac{1}{M_\Delta} \frac{d}{dx_\perp} \tilde{G}_1^{a'a}(x_\perp; P_z), \quad \rho_2(x_\perp; P_z) = -\frac{1}{3M_\Delta^2} x_\perp \frac{d}{dx_\perp} \frac{1}{x_\perp} \frac{d}{dx_\perp} \tilde{G}_2(x_\perp; P_z), \\ \rho_3(x_\perp; P_z) &= \frac{1}{M_\Delta^3} x_\perp^2 \frac{d}{dx_\perp} \frac{1}{x_\perp} \frac{d}{dx_\perp} \frac{1}{x_\perp} \frac{d}{dx_\perp} \tilde{G}_3(x_\perp; P_z). \end{aligned} \quad (26)$$

The variable  $\theta_{x_\perp}$  denotes the 2D angle of the  $x_\perp^i$ . Here we have used the 2D Fourier transform of the generic function  $F = \{G_0, G_0^{a'a}, G_1, G_1^{a'a}, G_2, G_3\}$ :

$$\int \frac{d^2 q_\perp}{(2\pi)^2} e^{-i\vec{q}_\perp \cdot \vec{x}_\perp} F(t; P_z) = \tilde{F}(x_\perp; P_z), \quad (27)$$

where we define the following functions for convenience

$$\begin{aligned} G_0(t; P_z) &= \left\{ G_{E0}(t; P_z) - \frac{2}{3} \tau G_{E2}(t; P_z) \right\}, \quad G_0^{a'a}(t; P_z) = \left\{ G_{E0}^{a'a}(t; P_z) + \frac{4}{3} \tau G_{E2}(t; P_z) \right\}, \\ G_1(t; P_z) &= \left\{ G_{E1}(t; P_z) - \frac{2}{5} \tau G_{E3}(t; P_z) \right\}, \quad G_1^{a'a}(t; P_z) = \left\{ G_{E1}^{a'a}(t; P_z) + \tau G_{E3}(t; P_z) \right\}, \\ G_2(t; P_z) &= G_{E2}(t; P_z), \quad G_3(t; P_z) = G_{E3}(t; P_z). \end{aligned} \quad (28)$$

Thus, one can clearly see that the multipole patterns  $\rho_{\text{mon}}, \rho_{\text{dip}}, \rho_{\text{quad}}$ , and  $\rho_{\text{oct}}$  of the charge distributions are given by the combinations of the  $\rho_0, \rho_1, \rho_2$ , and  $\rho_3$ .

### III. NUMERICAL RESULTS AND DISCUSSIONS

In this Section, We present the numerical results of the transverse charge distribution of the spin-3/2 baryon and discuss them. We consider those of  $\Delta^+$  and  $\Delta^0$ , regarding them as representatives for a spin-3/2 baryon. To study the charge distribution in the Wigner phase-space perspective, we need information on the  $\Delta$  EM form factors. While there is a plenty of available experimental data on the EM form factors of the nucleon, those of the  $\Delta$  baryons are almost unexplored on the experimental side due to their short-lived nature. One could import the lattice data [19] but they did not consider the EM form factors of the  $\Delta^0$ , of which the transverse charge distribution undergo a remarkable change under the Lorentz boost as in the case of the neutron [6, 35]. Thus, we will take the results from the SU(3) chiral quark-soliton model ( $\chi$ QSM) [43], where the available data of the EM form factors of the baryon decuplet exist. Note that the electric monopole, quadrupole, and magnetic dipole were calculated in the  $\chi$ QSM, but the magnetic octopole was ignored. This form factor is strongly suppressed in the large  $N_c$  expansion, which is consistent with the lattice QCD data on the  $G_{M3}$  form factor [19]. It is compatible with zero within the statistical accuracy.

In Fig. 1, we show the  $y$ -axis profiles of the transverse charge distribution of the moving  $\Delta^+$  baryon with the longitudinal momentum  $P_z$  varied from  $P_z = 0$  to  $P_z = \infty$ . Its spin is polarized along the  $z$ -axis with  $s_z = 3/2$  and  $s_z = 1/2$ , respectively. Taking  $P_z = 0$ , we obtain the 2D BF charge distribution. Here one should keep in mind that the 2D BF distribution is distinctive from the 3D one [40]. By carrying out the Abel transformation, one can project out the 2D distribution from the 3D one. In the projection, the quadrupole structure induces the monopole contribution, so the monopole charge distribution is subjected to the quadrupole contribution [40, 48]. In addition, this projection brings about the spin-polarization dependence of the monopole charge distribution. In addition, under the Lorentz boost, the transverse charge distributions with  $s_z = 1/2$  and  $s_z = 3/2$  are altered in a different manner. As demonstrated in Fig. 1,  $\rho_{\text{ch}}$  with  $s_z = 1/2$  changes stronger than that with  $s_z = 3/2$  as  $P_z$  increases.

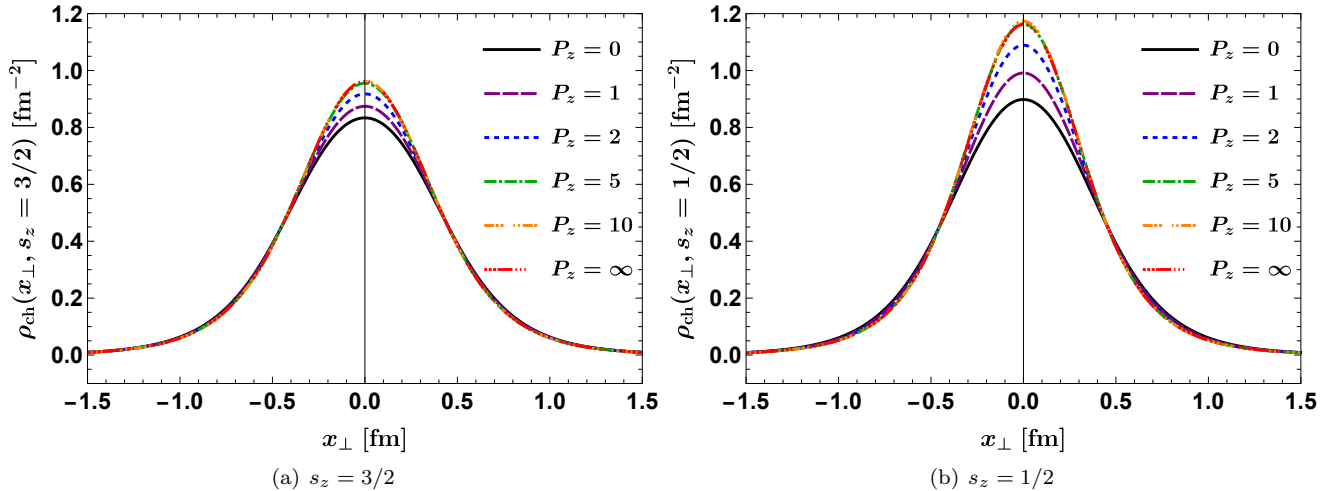


FIG. 1. The  $y$ -axis profiles of the transverse charge distributions of the moving  $\Delta^+$  baryon as the longitudinal momentum  $P_z$  increases from  $P_z = 0$  to  $P_z = \infty$ . Its spin is polarized along the  $z$ -axis with  $s_z = 3/2$  and  $s_z = 1/2$ , respectively. In the left (right) panel,  $\rho_{\text{ch}}$  with  $s_z = 3/2$  ( $s_z = 1/2$ ) is depicted.

In Fig. 2, we draw the  $y$ -axis profiles of the transverse charge distributions of the moving  $\Delta^0$  baryon as  $P_z$  increases from  $P_z = 0$  to  $P_z = \infty$ . Again, its spin is polarized along the  $z$ -axis with  $s_z = 3/2$  and  $s_z = 1/2$ , respectively. We observe that the relativistic effects (or Lorentz-boost effects) are prominent in the neutral  $\Delta^0$  baryon. Note that the transverse charge distribution of the neutral  $\Delta^0$  is normalized to its zero charge. It indicates that  $\rho_{\text{ch}}$  must at least have one nodal point. For the  $s_z = 3/2$ , the charge distribution spread widely and its nodal point is placed at a distance. As  $P_z$  increases from  $P_z = 0$  to  $P_z = \infty$ , the core part of the charge distribution gets weaker, whereas the tail part slowly gets lessened. So, the nodal point moves away to the outer part of the baryon. When it comes to  $s_z = 1/2$ , the configuration of the transverse charge distribution is dramatically changed under the Lorentz boost. In the rest frame ( $P_z = 0$ ), the center of the  $\Delta^0$  baryon is positively charged, whereas the outer part is negatively charged. When the system is boosted, the positive core gets weaker and then turns negative at around  $P_z \sim 2.8$  GeV. It is very similar to the behavior of the transverse neutron charge distribution under the Lorentz boost [35].

If the baryon is longitudinally polarized, then one can get access to the electric monopole and quadrupole form factors only. To see the additional contributions from the other form factors, the spin of the  $\Delta$  baryon should be

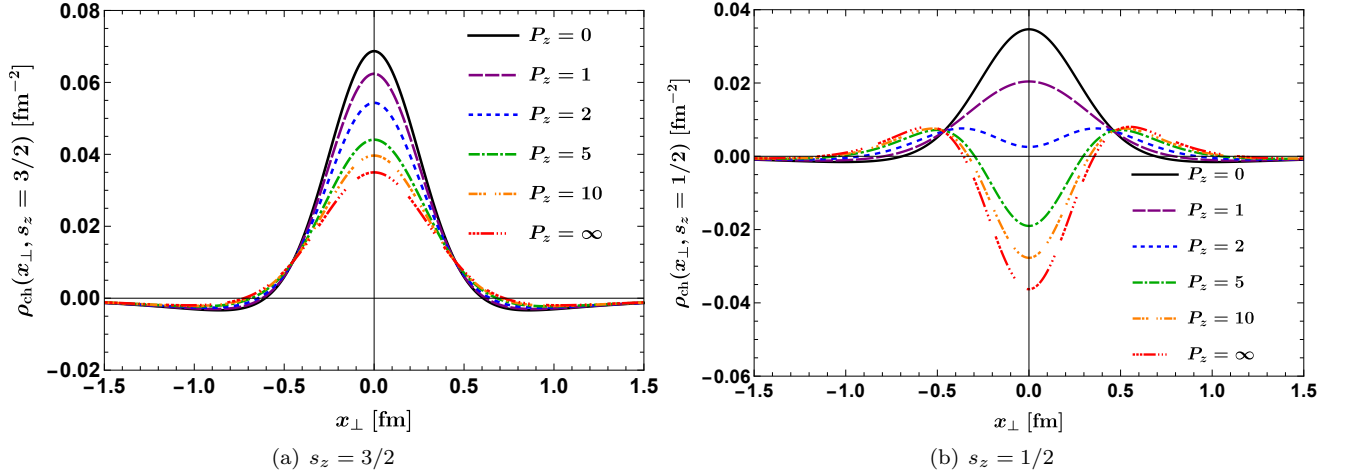


FIG. 2. The  $y$ -axis profiles of the transverse charge distributions of the moving  $\Delta^0$  baryon as the longitudinal momentum  $P_z$  increases from  $P_z = 0$  to  $P_z = \infty$ . Its spin is polarized along the  $z$ -axis with  $s_z = 3/2$  and  $s_z = 1/2$ , respectively. In the left (right) panel,  $\rho_{\text{ch}}$  with  $s_z = 3/2$  ( $s_z = 1/2$ ) is depicted.

polarized transversely. We express the transverse spin basis  $s_x$  in terms of the  $s_z$  basis. Then the spin states  $s_x = 1/2$  and  $s_x = 3/2$  are given [19] by

$$\begin{aligned}
 |s_x = 3/2\rangle &= \frac{1}{\sqrt{8}} \left( |s_z = 3/2\rangle + \sqrt{3}|s_z = 1/2\rangle + \sqrt{3}|s_z = -1/2\rangle + |s_z = -3/2\rangle \right), \\
 |s_x = 1/2\rangle &= \frac{1}{\sqrt{8}} \left( \sqrt{3}|s_z = 3/2\rangle + |s_z = 1/2\rangle - |s_z = -1/2\rangle - \sqrt{3}|s_z = -3/2\rangle \right).
 \end{aligned} \tag{29}$$

When the  $\Delta$  baryon is transversely polarized along the  $x$ -axis, its transverse charge distribution starts to get deformed as  $P_z$  increases. In the presence of the external magnetic field  $B$ , the electric dipole moment is induced by the moving  $\Delta$  baryon, which produces the electric field  $\mathbf{E}'$  depending on the velocity  $v$  of the moving  $\Delta$ , i.e.,  $\mathbf{E}' = \gamma(\mathbf{v} \times \mathbf{B})$ . A similar feature was also observed in the case of the neutron [7]. In addition, the induced electric octupole moment is also caused by this relativistic motion and results in the deformed charge distribution with the octupole pattern, unlike the nucleon. Figures 3(a)-(d) depict the numerical results of the monopole, dipole, quadrupole, and octupole patterns of the  $\Delta$  baryon charge distribution, respectively, when the  $\Delta$  is polarized along the  $x$ -axis with  $s_x = 3/2$ . One can obviously see that while the higher multipole contributions are found to be marginal, the dipole contribution arises as the most dominant one to deform the transverse charge distribution. At the rest frame, the dipole contribution is null, so the charge distribution is symmetric with respect to  $y = 0$ . Once the  $\Delta$  is boosted, the dipole contribution starts to increase and reaches its maximum value at around  $P_z \sim 1.4$  GeV. Then it diminishes gradually. At  $P_z \sim 10$  GeV, the size of the dipole contribution arrives at the minimum and then it starts to increase again but its sign is reversed (see Fig. 3(b)).

In the rest frame, the quadrupole contribution survives and makes the transverse charge distribution broaden. If the  $\Delta$  is boosted, the positive quadrupole contribution turns negative at around  $P_z \sim 1.4$  GeV. Figure 3(e) draws the charge distribution of the  $\Delta^+$  baryon with  $s_x = 3/2$ , which is the sum of Figs. 3(a)-(d). As shown in Fig. 3(e), the transverse charge distribution starts to be tilted to the positive  $x_\perp$ -direction till  $P_z = 1.4$  GeV and becomes symmetric with respect to  $x_\perp = 0$  at around  $P_z \sim 10$  GeV again. When  $P_z$  increases more, the charge distribution starts to move to the left  $x_\perp$ -direction. In the IMF ( $P_z = \infty$ ), we obtain the  $\Delta^+$  charge distribution with  $s_x = 3/2$  shifted to the left direction, which is consistent with the results from the lattice QCD [19]. Note that the induced electric dipole moment of the proton is defined as  $G_{M1}^N(0) - G_{E0}^N(0) > 0$ , whereas that of the  $\Delta$  baryon is proportional to  $G_{M1}^\Delta(0) - 3G_{E0}^\Delta(0) < 0$ , so that charge distribution of the  $\Delta^+$  is shifted to the left, which is opposite to the transverse proton charge distribution (see also Ref. [19]).

In Figs. 4(a)-(d) we present the numerical results for the monopole, dipole, quadrupole, and octupole patterns of the transverse  $\Delta^+$  charge distribution when it is polarized along the  $x$ -axis with  $s_x = 1/2$ . The sum of the total contributions is drawn in Fig. 4(e). They show a tendency similar to the  $s_x = 3/2$  case. However, the strength of the dipole contribution is almost a half of that with  $s_x = 3/2$ . So, the shape of the charge distribution is almost kept to be symmetric, and in the IMF they are shifted to the negative  $x_\perp$ -direction with respect to  $x_\perp = 0$ , which is also consistent with the results from Ref. [19].



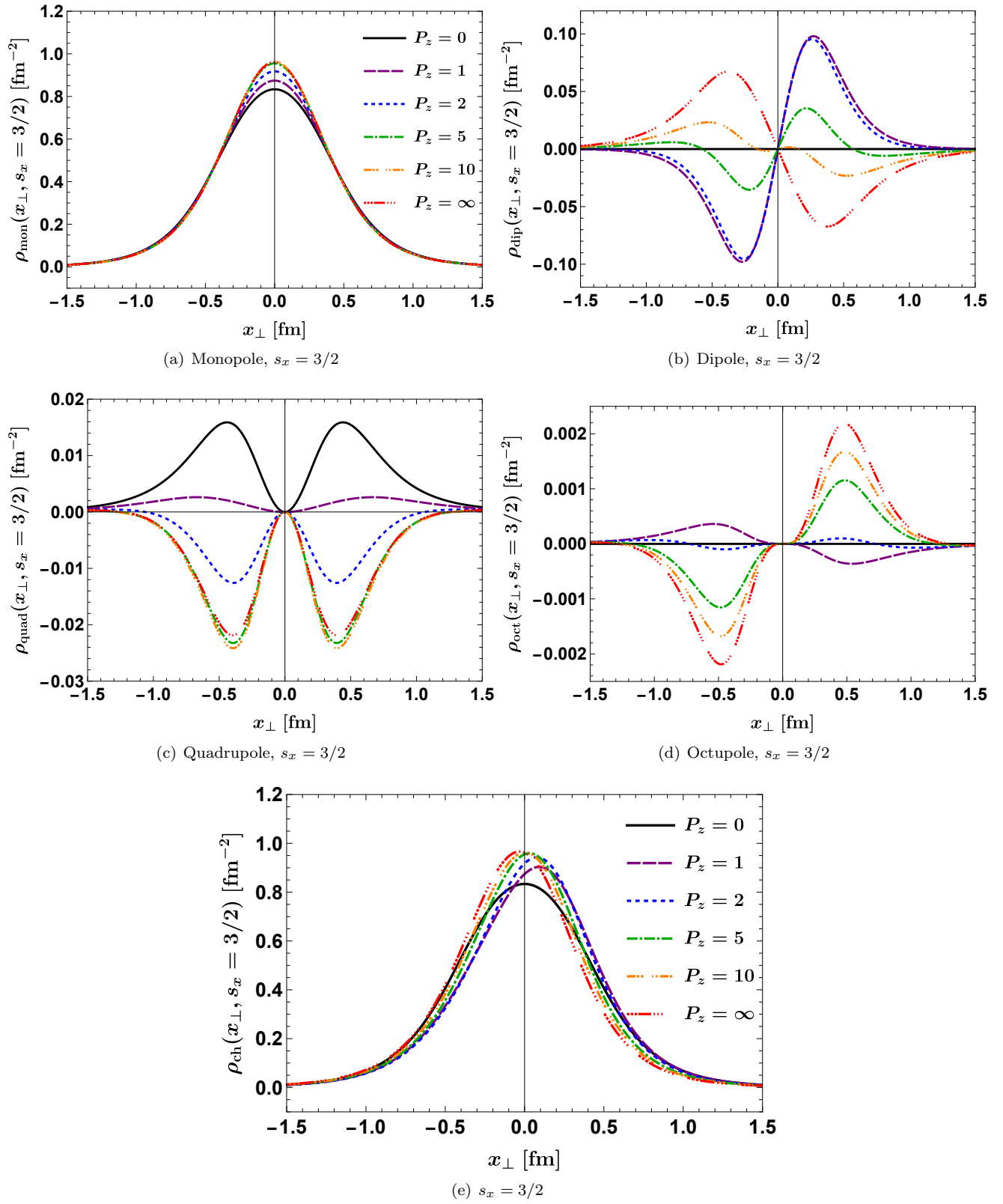


FIG. 3. (a) Monopole, (b) dipole, (c) quadrupole, and (d) octupole contributions to the  $y$ -axis profiles of the (e) transverse charge distributions of the  $\Delta^+$  baryon when its spin is polarized along the  $x$ -axis with  $s_x = 3/2$ .

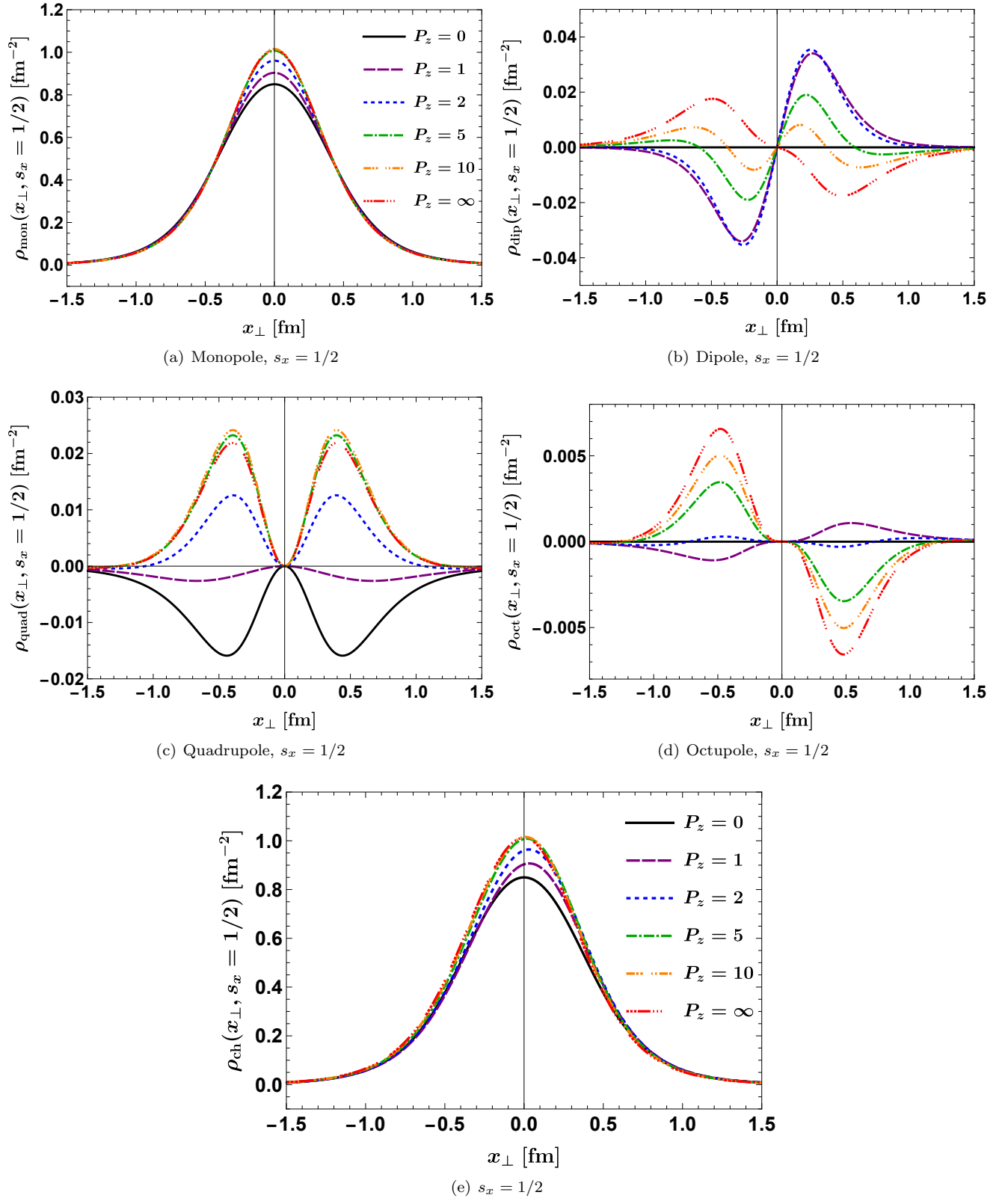


FIG. 4. (a) monopole, (b) dipole, (c) quadrupole, and (d) octupole contributions to the  $y$ -axis profiles of the (e) 2D charge distributions of the  $\Delta^+$  baryon when its spin is polarized along the  $x$ -axis with  $s_x = 1/2$ .

In the upper panel of Fig. 5, we illustrate the transverse charge distributions of the moving  $\Delta^+$  baryon transversely polarized along the  $x$ -axis with  $s_x = 3/2$ . As shown in Fig. 3 and Fig. 4, the charge distribution is deformed along the  $y$ -axis due to the presence of the quadrupole contribution, so that it is not spherically symmetric. Of course, there are no induced electric dipole and octupole contributions. The first column in Fig. 6 (Figs. 6(a), 6(e), 6(i), and 6(m)) shows the separate multipole contributions when the  $\Delta^+$  is at rest. Since the electric dipole moment is induced as the  $\Delta^+$  baryon is boosted along the  $z$ -axis, the transverse charge distribution starts to get deformed. At around  $P_z = 2$  GeV, the charge distribution is shifted to the positive  $x_\perp$ -axis due to the induced dipole contribution. On the other hand, the quadrupole contribution is relatively small in comparison with the dipole one. One of the remarkable features is that the sign of the quadrupole contribution is reversed at around  $P_z \sim 1.4$  GeV. See the second column in Fig. 6 (Figs. 6(b), 6(f), 6(j), and 6(n)). However, when the system is boosted larger than  $P_z \sim 10$  GeV, the sign of the induced dipole contribution is reversed, so the charge distribution is moved to the opposite direction, while the higher multipoles contribute marginally to the charge distribution. In the IMF, however, the quadrupole contribution dominates over the dipole contribution. See the last column in Fig. 6 (Figs. 6(d), 6(h), 6(l), and 6(p)). When it comes to the  $s_x = 1/2$ , the tendency is almost the same as the case of  $s_x = 3/2$ , but the quadrupole contribution has the opposite sign at the rest frame. So, the charge distribution broadens along the  $x$ -axis instead of the  $y$ -axis. See the first column in Fig. 7 (Figs. 7(a), 7(e), 7(i), and 7(m)).

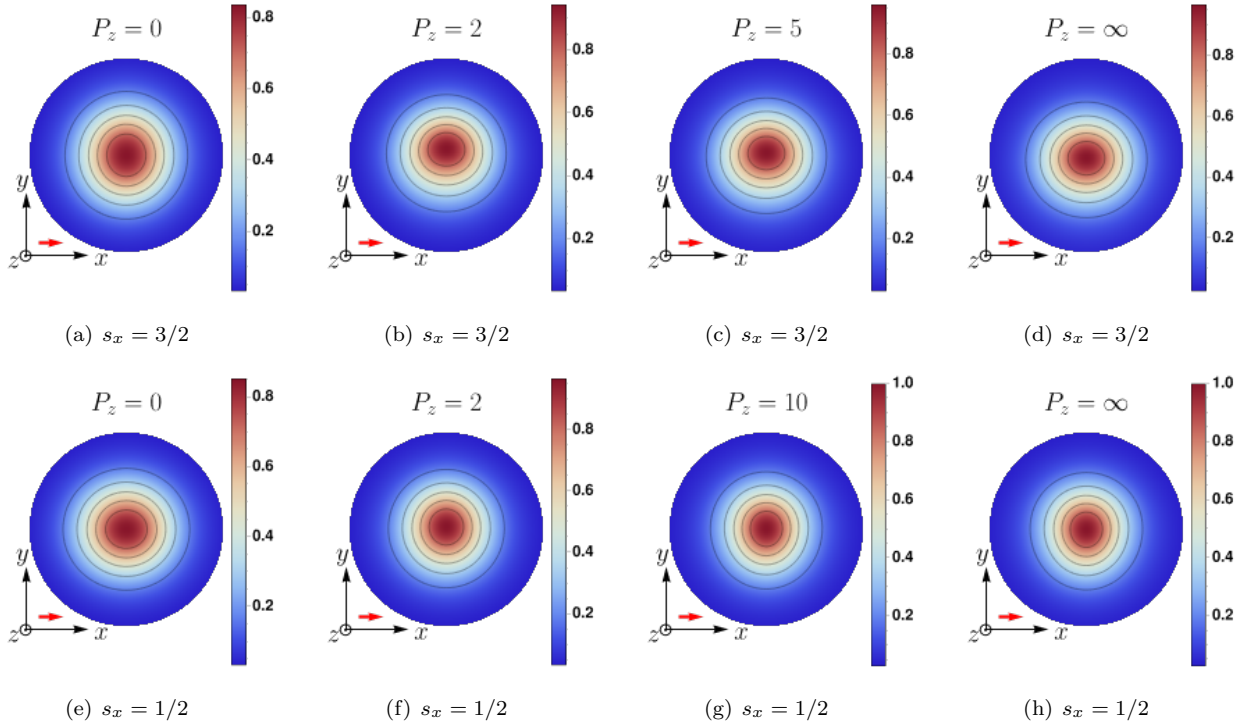


FIG. 5. (a)-(d) 2D charge distributions of the moving  $\Delta^+$  baryon transversely polarized along  $x$ -axis with  $s_x = 3/2$ ; (e)-(h) 2D charge distributions of the moving  $\Delta^+$  baryon transversely polarized along  $x$ -axis with  $s_x = 1/2$

We also examine how the transverse charge distribution of the  $\Delta^0$  baryon transversely polarized along the  $x$ -axis varies under the Lorentz boost. In Fig. 8, we draw the transverse charge distributions of the  $\Delta^0$  baryon when its spin is polarized along the  $x$ -axis with  $s_x = 3/2$ . See Fig. 8 (Figs. 8(a)-(e)). We found that the transverse  $\Delta^0$  charge distribution is dramatically changed under the Lorentz boost, in contrast with that of the  $\Delta^+$  baryon. At the rest frame, the monopole contribution is positive at the inner part, whereas the quadrupole contribution is negative over  $r$ . Obviously, there are no induced dipole and octupole contributions. So, while the transverse charge distribution is kept to be positive at the core part, the quadrupole contribution pulls it down to be negative at the outer part. As a result, the nodal point of the transverse charge distribution gets close to the center of the  $\Delta^0$  baryon due to the quadrupole contribution. As  $P_z$  increases, the charge distribution starts to be deformed. The dominant contribution to  $\rho_{\text{ch}}(x_\perp)$  is the monopole one, and it is always kept to be positive at the core part. As we explained before, the monopole contribution to the transversely polarized charge distribution under the Lorentz boost turns out to be always positive at the core part, though there is a sign flip of the longitudinally polarized charge distribution. The quadrupole contribution turns positive at around  $P_z \sim 4.0$  GeV at the core part. At the same moment, the induced dipole

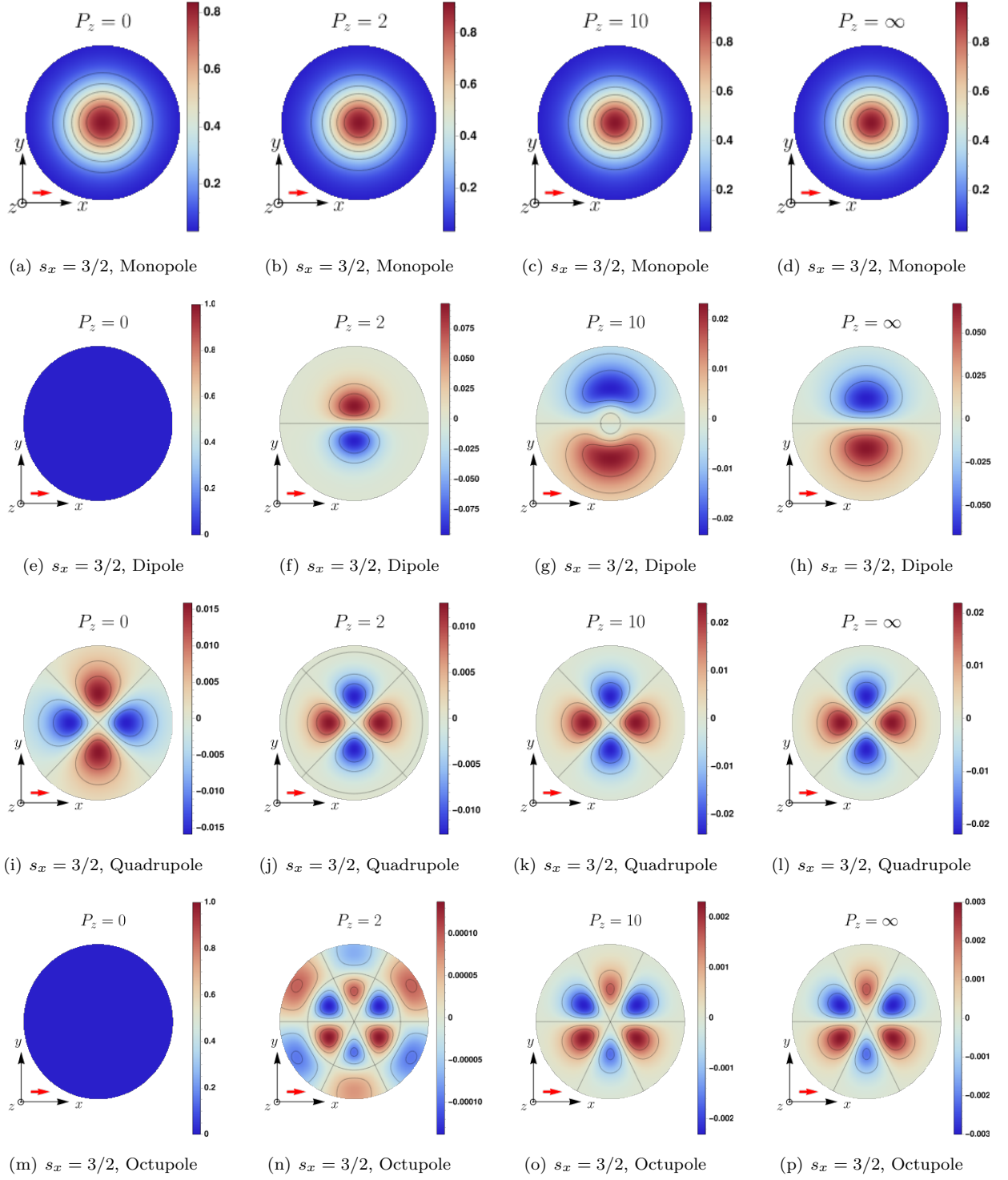


FIG. 6. (a)-(d) monopole, (e)-(h) dipole, (i)-(l) quadrupole, and (m)-(p) octupole contributions of  $\Delta^+$  with  $s_x = 3/2$  to the 2D charge distribution.

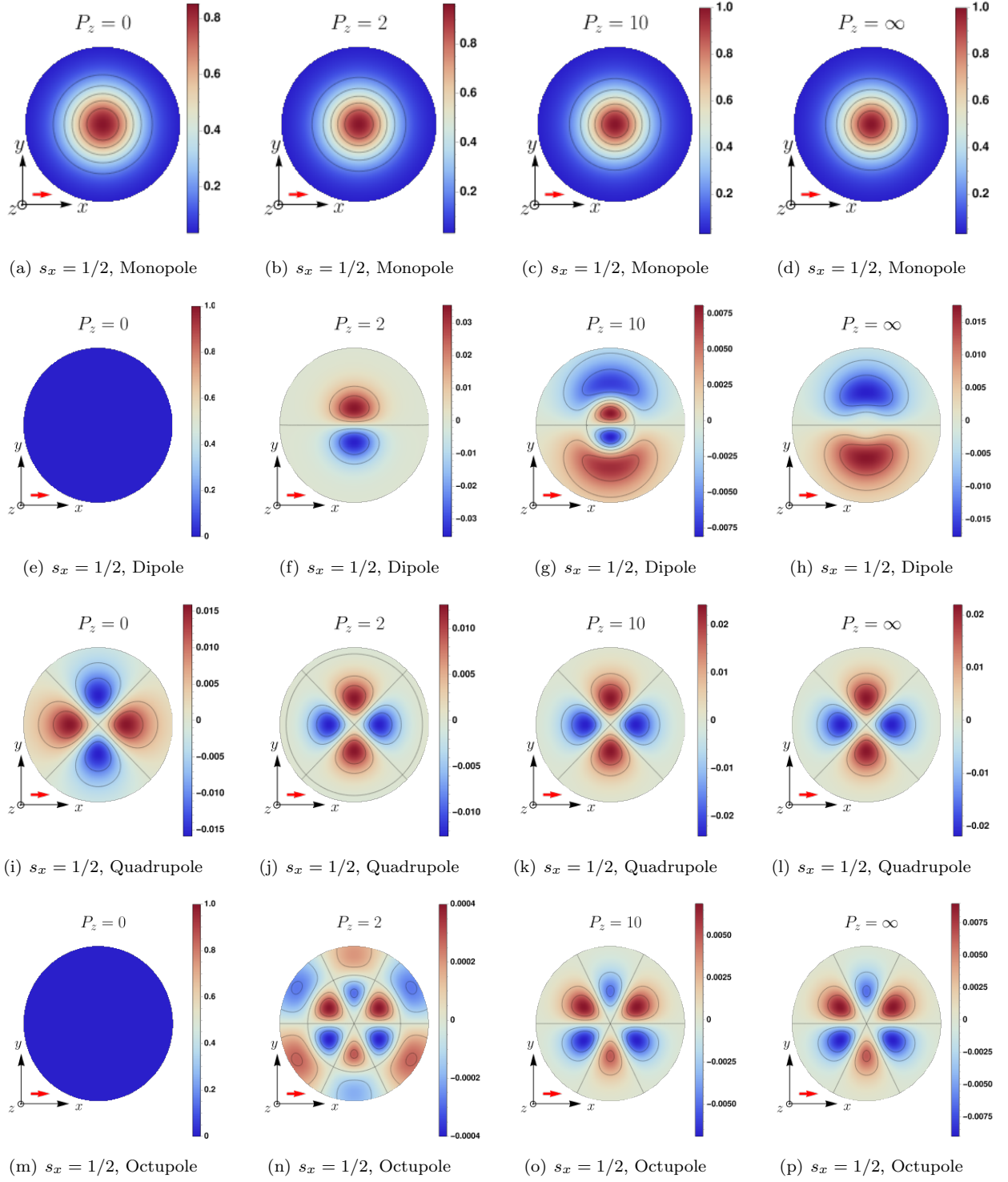


FIG. 7. (a)-(d) monopole, (e)-(h) dipole, (i)-(l) quadrupole, and (m)-(p) octupole contributions of  $\Delta^+$  with  $s_x = 1/2$  to the 2D charge distribution.

contribution pushes the charge distribution to the negative  $y$ -direction, which dominates over the higher multipole contributions. The value of the  $G_{M1}^{\Delta^0}(0) \sim -0.3\mu_N$  [43] is solely governed by the induced dipole moment because of the  $G_{E0}^{\Delta^0}(0) = 0$ . This is the reason why the transverse charge distribution of the  $\Delta^0$  is deformed as that of the neutron, i.e.,  $G_{M1}^n(0) = -1.91\mu_N$  [49], as shown in Fig. 8(e).

In the IMF, we finally obtain the transverse charge distribution shifted to the negative  $y$ -axis. When the spin projection is  $s_x = 1/2$ , we are able to see that quadrupole contribution is opposite to the  $s_x = 3/2$  case in the rest frame. See Fig. 9 (Fig. 9(a)-(d)). The quadrupole contribution makes a rather weak plateau at the core part of the charge distribution, which is a similar feature to the deuteron charge distribution [25, 40]. When the system is boosted, the quadrupole contribution is relatively suppressed and the induced dipole contribution dominates over it. In the IMF, we obtained the  $\Delta^0$  charge distribution  $s_x = 1/2$ , which has a similar shape and strength to that with  $s_x = 3/2$ .

In the upper panel of Fig. 10, we draw the 2D charge distributions of the moving  $\Delta^0$  baryon transversely polarized along the  $x$ -axis with  $s_x = 3/2$ . As shown in Fig. 8 and Fig. 9, the charge distribution is squeezed along the  $y$ -axis due to the presence of the quadrupole contribution at the rest frame. See the first column in Fig. 11 (Figs. 11(a), 11(e), 11(i), and 11(m)). If the  $\Delta^0$  baryon starts to move along the  $z$ -axis, the electric dipole is induced and deforms the charge distribution. So, the charge distribution starts to be tilted to the negative  $y$ -direction, and the dipole contribution is saturated to  $G_M^{\Delta^0} \sim -0.3$  in the IMF. Together with the quadrupole and octupole contributions, we obtained a rather complicated structure of the charge distribution of the  $\Delta^0$  with  $s_x = 3/2$  in the IMF in Fig. 10. When it comes  $s_x = 1/2$ , the tendency is almost kept to be the same as  $s_x = 3/2$ , but the opposite sign of the quadrupole contribution squeezes the charge distribution along  $x$ -axis instead of  $y$ -axis at the rest frame. See the first column in Fig. 12 (Figs. 12(a), 12(e), 12(i), and 12(m)).

#### IV. SUMMARY AND CONCLUSIONS

In the present work, we aimed at investigating how the transverse charge distributions of both the unpolarized and transversely polarized  $\Delta$  baryon change under the Lorentz boost from  $P_z = 0$  to  $P_z = \infty$  in the Wigner phase-space perspective. We first observed that the elastic frame naturally interpolates the transverse charge distributions between the Breit frame and infinite momentum frame, even for the spin-3/2 particle. In this elastic frame, the transverse charge distributions acquire four different contributions: the monopole, quadrupole, induced dipole, and induced octupole contributions. To visualize them in the 2D space, we employed the electromagnetic form factors of the  $\Delta$  baryon extracted from the SU(3) chiral quark-soliton model. The Lorentz boost and the geometrical projection from the 3D to 2D spaces yield a split in the spin-polarization of the monopole and induced dipole contributions. When both the  $\Delta^+$  and  $\Delta^0$  baryons are polarized along the  $z$ -axis, we found that their charge distributions are always kept to be spherically symmetric under the Lorentz boost. For the  $\Delta^0$ , the shape of the transverse charge distribution was dramatically changed under the Lorentz boost, which is similar to the neutron case. When the  $\Delta$  baryon is transversely polarized along the  $x$ -axis, all the multipole structures start to appear. In the rest frame, the quadrupole contribution does not vanish and makes the charge distribution deformed. When  $P_z$  increases, the dipole and octupole contributions are induced and cause the asymmetry of the transverse charge distribution. For the  $\Delta^+$  baryon with  $s_x = 1/2$  and  $s_x = 3/2$ , the charge distributions start to be shifted to the positive  $y$ -direction and reach the maximal values of the electric dipole moments at around  $P_z \sim 1.4$  GeV and gradually diminish. They turn negative at around  $P_z = 10$  GeV. As a result, the transverse charge distributions of the transversely polarized  $\Delta^+$  baryon along the  $x$ -axis is moved to the negative  $y$ -direction in the infinite momentum frame. We found that these results are consistent with the results from the lattice QCD for the  $\Delta^+$ . For the  $\Delta^0$  baryon, the positive charges, which represent the up quark inside the  $\Delta^0$  baryon, were displaced to the negative  $y$ -direction whereas the negative charges or the down quarks were moved toward the positive  $y$ -direction. This is due to the negative values of the electric dipole moment ( $G_{M1}^{\Delta^0} \sim -0.3$ ) of the  $\Delta^0$  baryon.

#### ACKNOWLEDGMENTS

This material is based upon work supported by the U.S. Department of Energy, Office of Science, Office of Nuclear Physics under contract DE-AC05-06OR23177 (J.-Y. Kim), and by the Basic Science Research Program through the National Research Foundation of Korea funded by the Korean government (Ministry of Education, Science and Technology, MEST), Grant-No. 2021R1A2C2093368 and 2018R1A5A1025563.

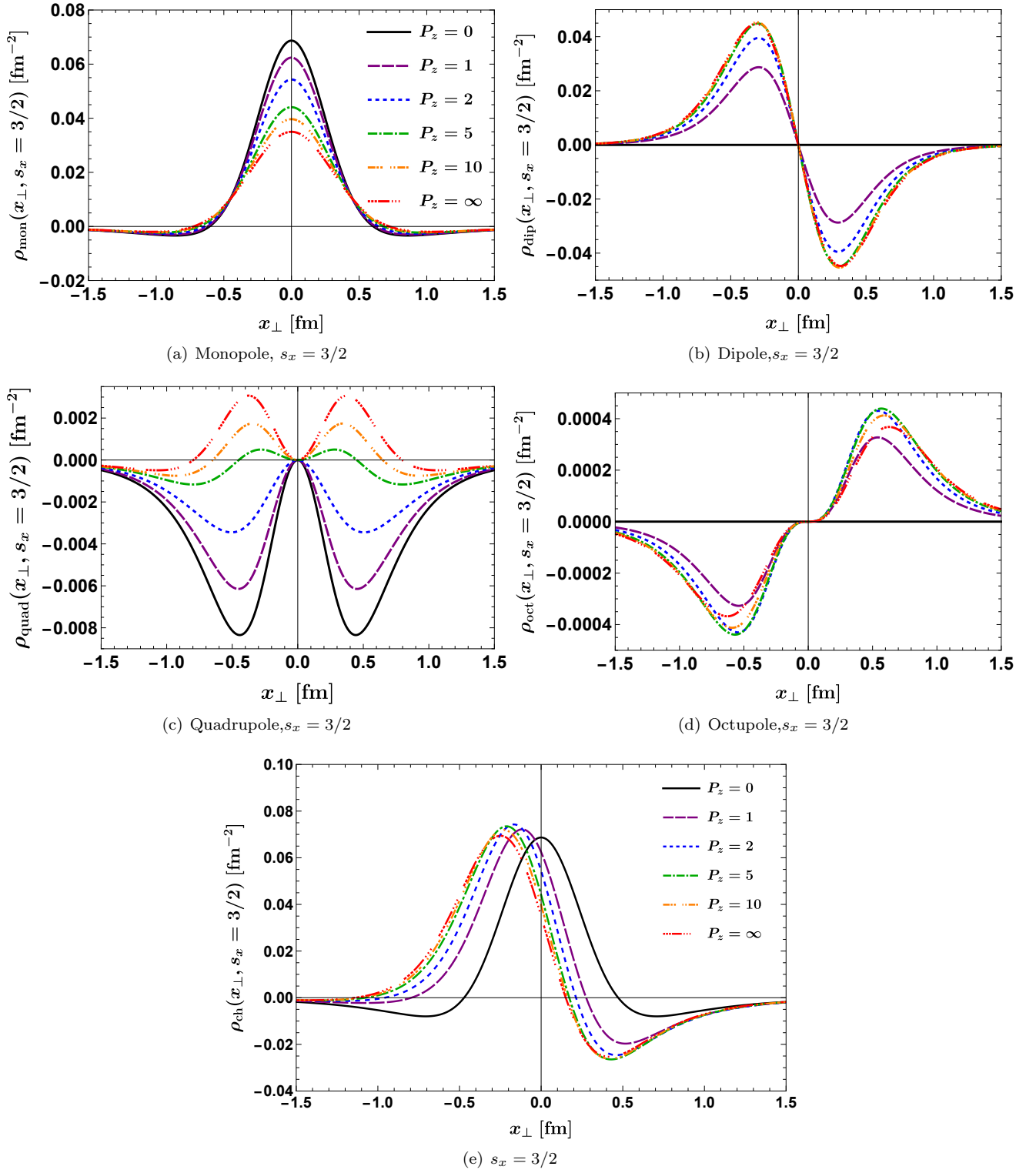


FIG. 8. (a) Monopole, (b) dipole, (c) quadrupole, and (d) octupole contributions to the  $y$ -axis profiles of the (e) 2D charge distributions of the  $\Delta^0$  baryon when its spin is polarized along the  $x$ -axis with  $s_x = 3/2$ .

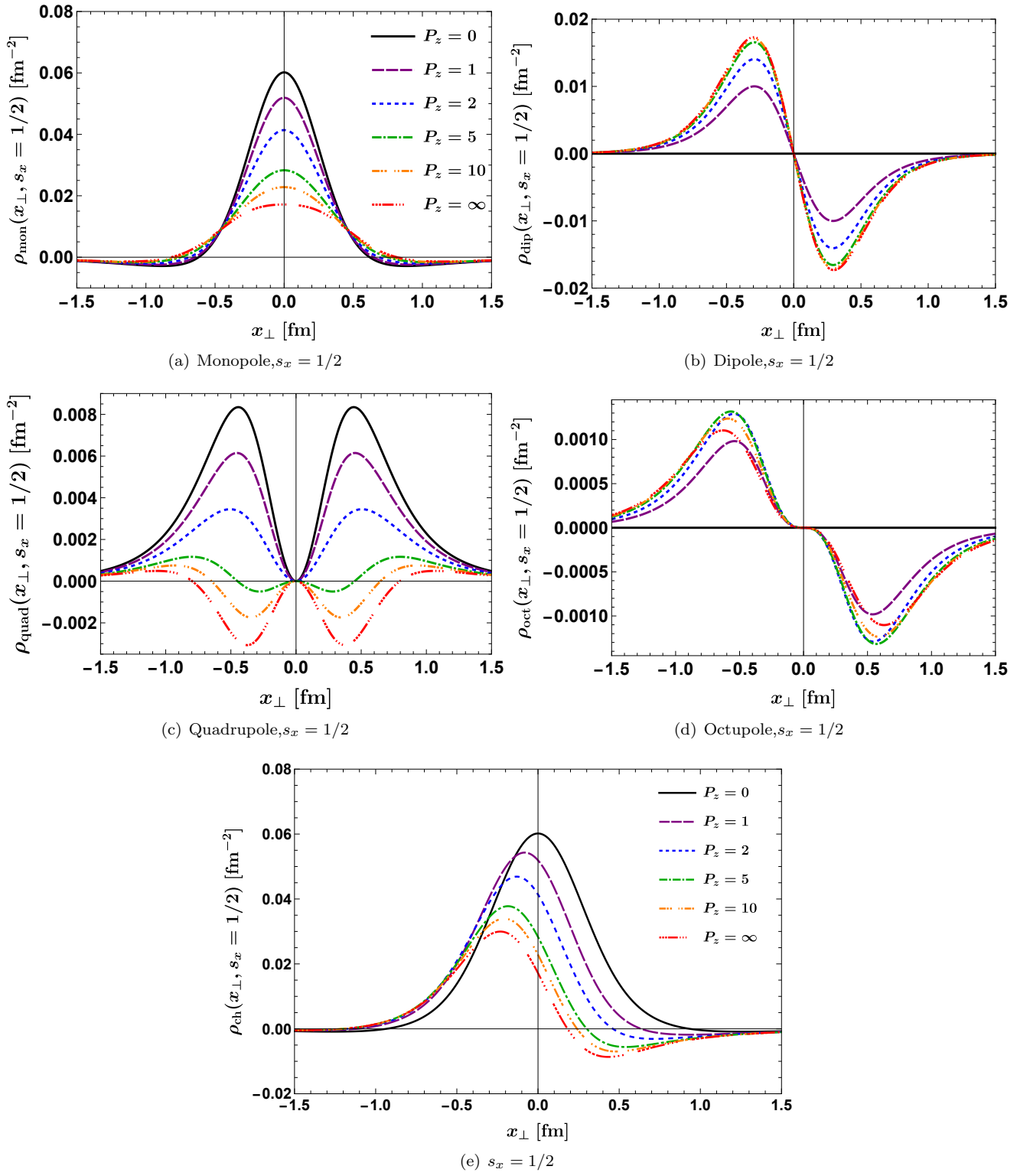


FIG. 9. (a) monopole, (b) dipole, (c) quadrupole, and (d) octupole contributions to the  $y$ -axis profiles of the (e) 2D charge distributions of the  $\Delta^0$  baryon when its spin is polarized along the  $x$ -axis with  $s_x = 1/2$



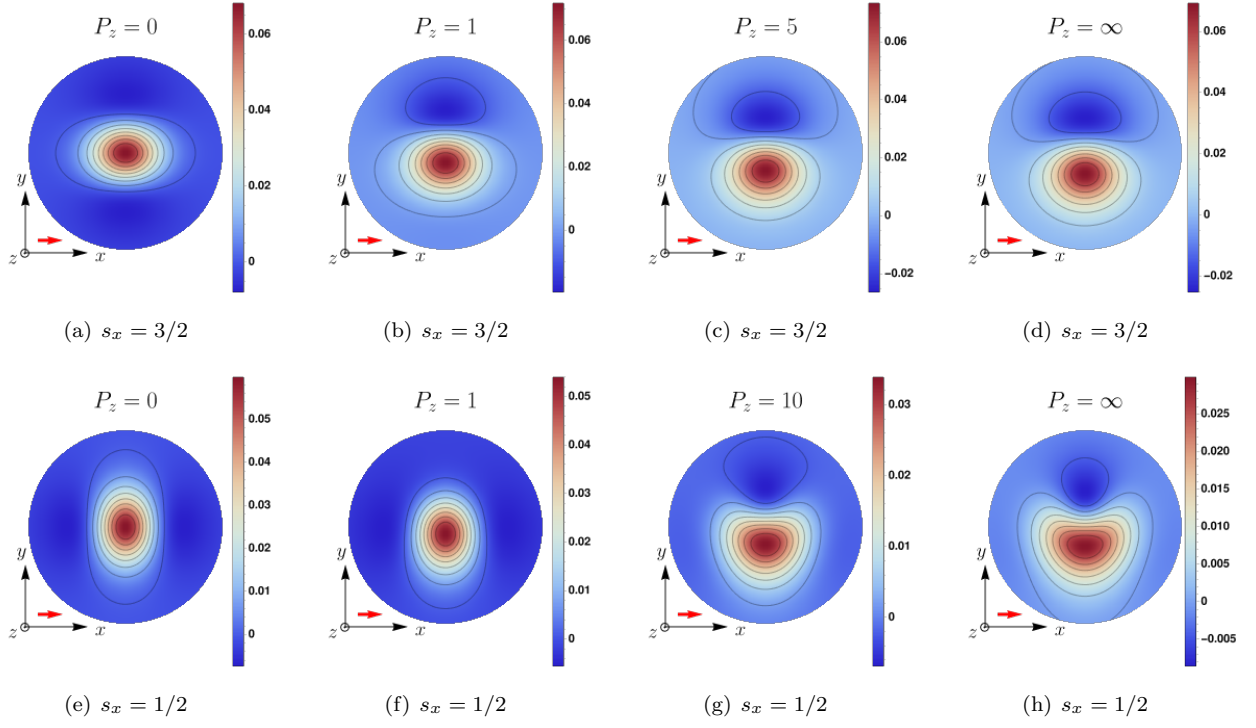


FIG. 10. (a)-(d) 2D charge distributions of the moving  $\Delta^0$  baryon transversely polarized along  $x$ -axis with  $s_x = 3/2$ ; (e)-(h) 2D charge distributions of the moving  $\Delta^0$  baryon transversely polarized along  $x$ -axis with  $s_x = 1/2$

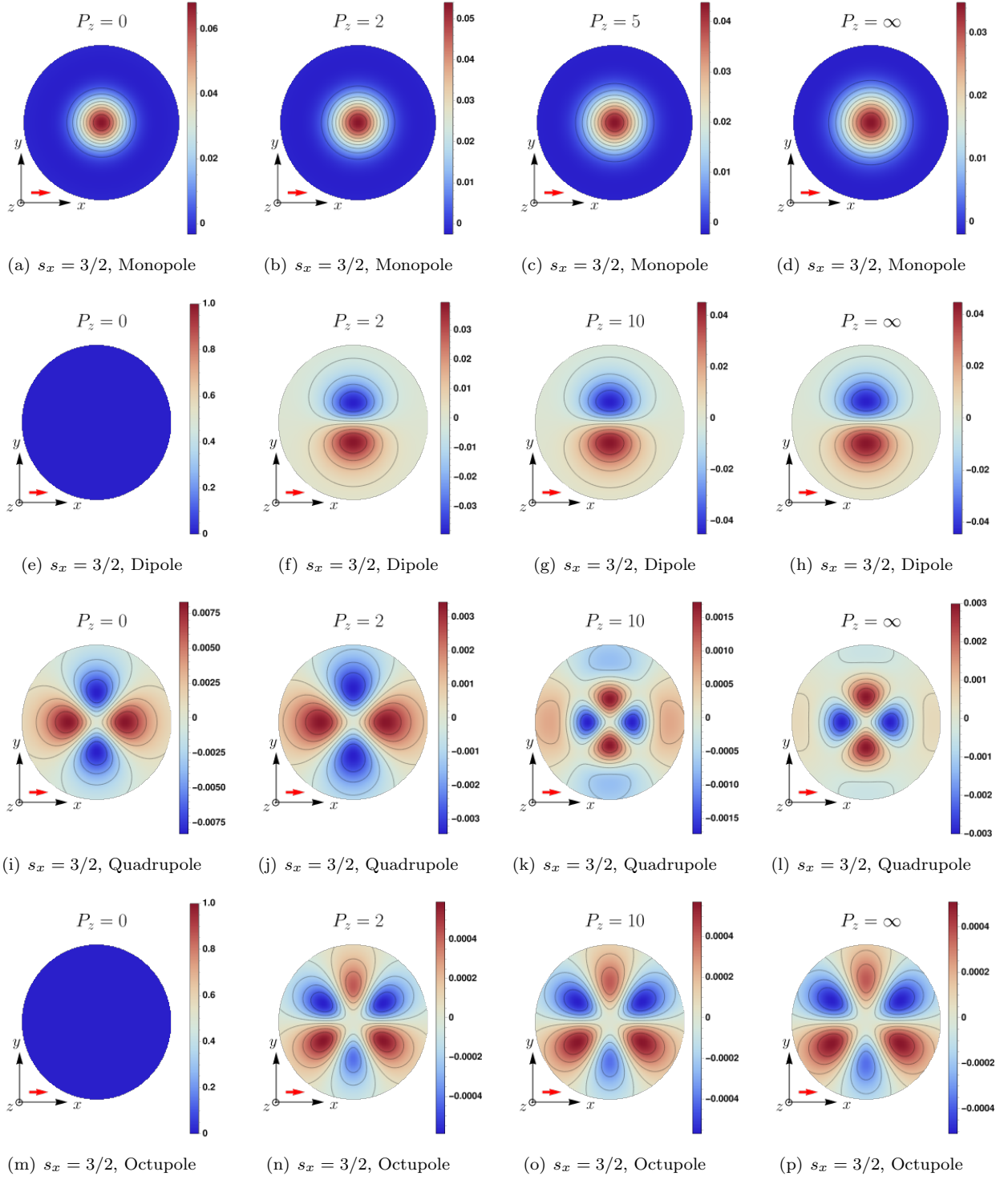


FIG. 11. (a)-(d) monopole, (e)-(h) dipole, (i)-(l) quadrupole, and (m)-(p) octupole contributions of  $\Delta^0$  with  $s_x = 3/2$  to the 2D charge distribution.

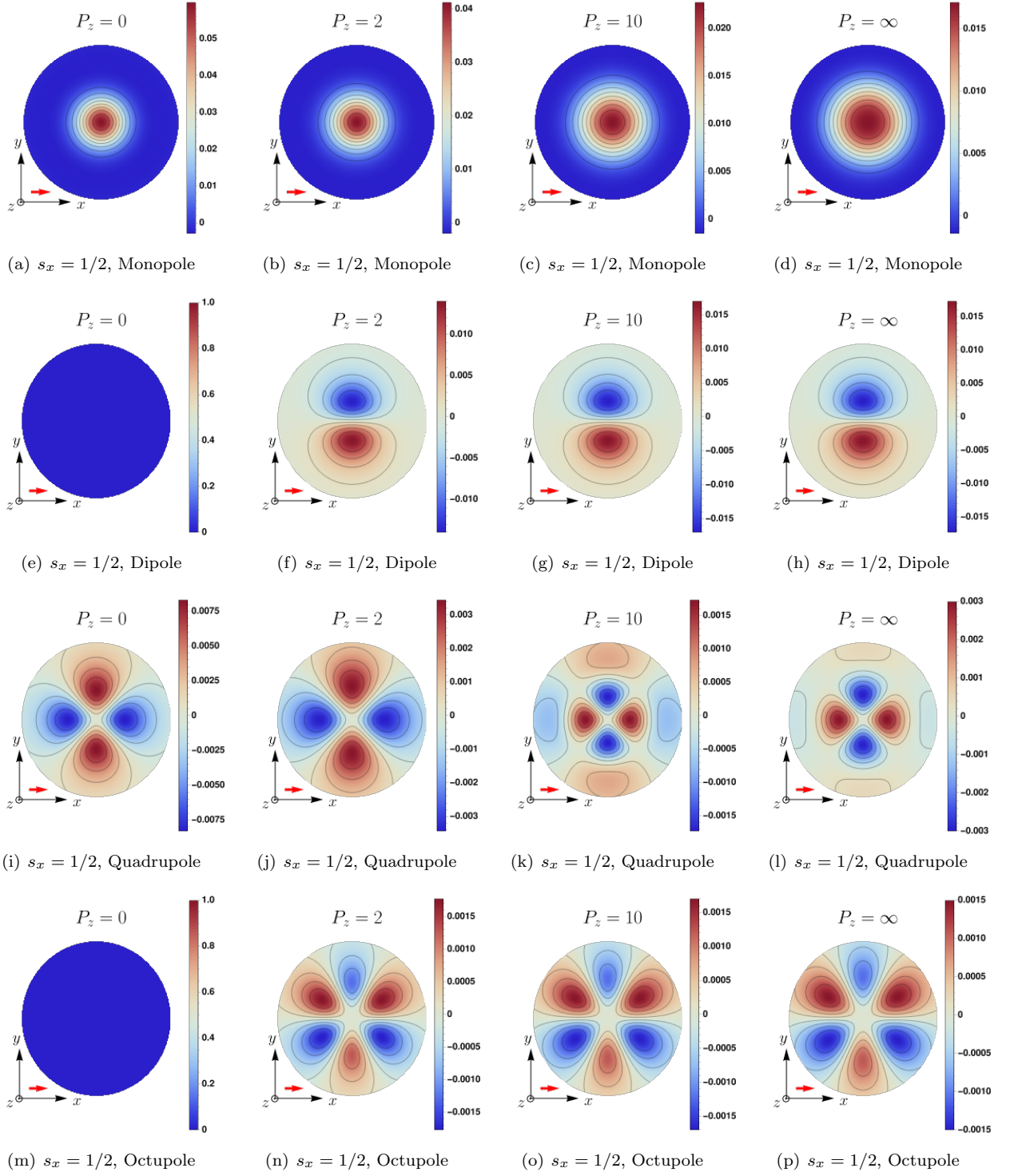


FIG. 12. (a)-(d) monopole, (e)-(h) dipole, (i)-(l) quadrupole, and (m)-(p) octupole contributions of  $\Delta^0$  with  $s_x = 1/2$  to the 2D charge distribution.

### Appendix A: frame-dependent functions

In this Appendix, We listed the explicit expressions of the frame-dependent functions for both temporal and spatial components of the EM current. To express them in a compact way, we introduce the following functions:

$$A = \frac{1}{M(M + P_0)}, \quad \beta_n^\perp = 1 + \frac{\vec{q}_\perp^2}{nM(M + P_0)}, \quad \beta_n^z = 1 + \frac{P_z^2}{nM(M + P_0)}. \quad (\text{A1})$$

All the frame-dependent functions appearing in the matrix element of the temporal component of the EM current are listed as follows:

$$\begin{aligned} G_{E0}(t; P_z) &= \frac{1}{2P_0} \left[ 2M \left( \beta_1^z - \frac{1}{3} At \beta_8^\perp \beta_1^z - \frac{1}{6} P_z^2 \beta_4^\perp t A^2 \right) F_1^*(t) + \frac{t F_2^*(t)}{2M} \left( 1 - \frac{1}{3} At \beta_8^\perp + \frac{2}{3} P_z^2 A \beta_4^\perp \right) \right. \\ &\quad \left. + \frac{\beta_4^\perp t F_3^*(t)}{6M} \left( \beta_1^z \beta_4^\perp - \frac{P_z^2 A^2 t}{4} \right) + \frac{\beta_4^\perp t^2 F_4^*(t)}{8M^3} \left( \frac{P_z^2 A}{3} + \frac{1}{3} \beta_4^\perp \right) \right] \\ G_{E0}^{a'a}(t; P_z) &= \frac{1}{2P_0} \left[ \frac{2}{3} M P_z^2 A^2 t (\beta_1^z - 2\beta_4^\perp) F_1^*(t) + \frac{P_z^2 t^2 A^2 F_3^*(t)}{12M} (\beta_1^z - 2\beta_4^\perp) \right. \\ &\quad \left. - \frac{P_z^2 At F_2^*(t)}{6M} (8\beta_4^\perp - At) - \frac{P_z^2 At^2 F_4^*(t)}{48M^3} (8\beta_4^\perp - At) \right] \\ G_{E1}(t; P_z) &= \frac{1}{2P_0} \left[ \frac{2P_z M^2 A F_1^*(t)}{3} \left( 1 - 2\beta_4^\perp \beta_1^z - \frac{2t A \beta_8^\perp}{5} \right) - \frac{P_z t A \beta_4^\perp F_3^*(t)}{12} \left( 2\beta_1^z - \frac{4\beta_4^\perp}{5} \right) \right. \\ &\quad \left. + \frac{P_z F_2^*(t)}{6} \left( 4 - 2At \beta_4^\perp - \frac{8At \beta_8^\perp}{5} \right) - \frac{P_z t \beta_4^\perp F_4^*(t)}{8M^2} \left( \frac{At}{3} - \frac{8}{15} \beta_4^\perp \right) \right] \\ G_{E1}^{a'a}(t; P_z) &= \frac{1}{2P_0} \left[ \frac{P_z^3 t M^2 A^3}{3} F_1^*(t) + \frac{P_z^3 A^3 t^2}{24} F_3^*(t) + \frac{P_z^3 A^2 t}{3} F_2^*(t) + \frac{P_z^3 t^2 A^2}{24M^2} F_4^*(t) \right] \\ G_{E2}(t; P_z) &= -\frac{3}{2P_0} \left[ \frac{2}{3} M^3 A (\beta_8^\perp \beta_1^z + P_z^2 A \beta_4^\perp) F_1^*(t) + \frac{M \beta_4^\perp F_3^*(t)}{12} (P_z^2 A^2 t - 2\beta_1^z \beta_4^\perp) \right. \\ &\quad \left. + \frac{M A F_2^*(t)}{6} (t \beta_8^\perp + 4P_z^2 \beta_4^\perp) + \frac{t F_4^*(t)}{24M} (2P_z^2 A \beta_4^\perp - \beta_4^{\perp 2}) \right] \\ G_{E3}(t; P_z) &= \frac{1}{2P_0} \left[ -\frac{2}{3} P_z \beta_8^\perp M^4 A^2 F_1^*(t) + \frac{1}{6} M^2 A F_3^*(t) P_z \beta_4^{\perp 2} - \frac{2}{3} P_z \beta_8^\perp M^2 A F_2^*(t) + \frac{1}{6} F_4^*(t) \beta_4^{\perp 2} P_z \right], \quad (\text{A2}) \end{aligned}$$

All the frame-dependent functions appearing in the matrix element of the spatial components of the EM current are listed as follows:

$$\begin{aligned}
G_{M0}^3(t; P_z) &= \frac{1}{2P_0} \left[ P_z(2 - tA\beta_6^\perp)F_1^* + \frac{P_z t\beta_4^\perp}{24M^2}(4\beta_4^\perp - tA)F_3^* + \frac{P_z tA}{6} \left( 1 - \frac{1}{2}At\beta_4^\perp + 2AP_z^2\beta_4^\perp \right) F_2^* \right. \\
&\quad \left. + \frac{P_z t^2 A^2 \beta_4^\perp}{24M^2} \left( P_z^2 - \frac{1}{4}t \right) F_4^* \right] \\
G_{M0}^{3,a'a}(t; P_z) &= \frac{1}{2P_0} \left[ \frac{2}{3}P_z^3 t A^2 F_1^* + \frac{P_z^3 t^2 A^2}{12M^2} F_3^* - \frac{4}{3}P_z^3 A^2 t \beta_{8/3}^\perp F_2^* - \frac{P_z^3 A^2 t^2 \beta_{8/3}^\perp}{6M^2} F_4^* \right] \\
G_{M1}^\perp(t; P_z) &= \frac{1}{2P_0} \left[ \frac{2}{3}M \left( 1 - \frac{2}{5}\beta_8^\perp tA \right) F_1^* + \frac{\beta_4^{\perp 2} t}{15M} F_3^* + \frac{1}{3}M \left( 1 - \frac{2}{5}tA\beta_8^\perp tA \right) (2\beta_2^z - P_z^2 A) F_2^* \right. \\
&\quad \left. + \frac{t\beta_4^{\perp 2} t}{30M} (2\beta_2^z - P_z^2 A) F_4^* \right] \\
G_{M1}^3(t; P_z) &= \frac{1}{2P_0} \left[ \frac{2}{3}M \left( 1 - 2P_z^2 A\beta_4^\perp - \frac{2}{5}\beta_8^\perp tA \right) F_1^* - \frac{\beta_4^\perp t}{6M} \left( P_z^2 A - \frac{2}{5}\beta_4^\perp \right) F_3^* \right. \\
&\quad \left. + \frac{M}{3} \left\{ P_z^2 A \left( 1 - \frac{7}{5}At\beta_{14/3}^\perp \right) + 2\beta_2^z \left( 1 - \frac{2}{5}tA\beta_8^\perp \right) \right\} F_2^* + \frac{\beta_4^\perp t}{30M} \left( P_z^2 A\beta_{2/3}^\perp + \beta_2^z \beta_4^\perp \right) F_4^* \right] \\
G_{M1}^{\perp,a'a}(t; P_z) &= \frac{1}{2P_0} \left[ \frac{2}{3}MP_z^2 A^2 t F_1^* + \frac{1}{12M} P_z^2 t^2 A^2 F_3^* + \frac{1}{3}MP_z^2 t A^2 (2\beta_2^z - P_z^2 A) F_2^* \right. \\
&\quad \left. + \frac{1}{48M} P_z^2 A^2 t^2 (2 + 2\beta_2^z - P_z^2 A) F_4^* \right] \\
G_{M1}^{3,a'a}(t; P_z) &= \frac{1}{2P_0} \left[ \frac{1}{3}MP_z^2 A^2 t F_1^* + \frac{1}{24M} P_z^2 t^2 A^2 F_3^* + \frac{1}{6}MP_z^2 A^2 t (2\beta_2^z + P_z^2 A) F_2^* \right. \\
&\quad \left. + \frac{1}{48M} P_z^2 t^2 A^2 (2\beta_2^z + P_z^2 A) F_4^* \right] \\
G_{M3}^\perp(t; P_z) &= \frac{1}{2P_0} \left[ -\frac{2}{3}M^3 \beta_8^\perp A F_1^* + \frac{1}{6}M\beta_4^{\perp 2} F_3^* - \frac{1}{3}M^3 A\beta_8^\perp (2\beta_2^z - P_z^2 A) F_2^* + \frac{1}{12}M\beta_4^{\perp 2} (2\beta_2^z - P_z^2 A) F_4^* \right] \\
G_{M3}^3(t; P_z) &= \frac{1}{2P_0} \left[ -\frac{2}{3}M^3 \beta_8^\perp A F_1^* + \frac{1}{6}M\beta_4^{\perp 2} F_3^* - \frac{1}{3}M^3 A\beta_8^\perp (2\beta_2^z + P_z^2 A) F_2^* + \frac{1}{12}M\beta_4^{\perp 2} (2\beta_2^z + P_z^2 A) F_4^* \right] \\
G_{M2}^\perp(t; P_z) &= \frac{1}{2P_0} \left[ \frac{2}{3}M^2 P_z A\beta_4^\perp F_1^* + \frac{1}{12}P_z A t \beta_4^\perp F_3^* + \frac{1}{3}P_z M^2 A\beta_4^\perp (2\beta_2^z - P_z^2 A) F_2^* \right. \\
&\quad \left. + \frac{1}{24}P_z t A\beta_4^\perp (2\beta_2^z - P_z^2 A) F_4^* \right] \\
G_{M2}^3(t; P_z) &= \frac{3}{2P_0} \left[ -\frac{2}{3}M^2 P_z A(\beta_4^\perp + \beta_8^\perp) F_1^* + \frac{1}{12}P_z \beta_4^\perp (2\beta_4^\perp - tA) F_3^* \right. \\
&\quad \left. - \frac{1}{3}M^2 P_z A \left( \frac{1}{2}At\beta_8^\perp + 2\beta_2^z \beta_4^\perp + P_z^2 A\beta_4^\perp \right) F_2^* + \frac{1}{24}P_z t A\beta_4^\perp (\beta_4^\perp - 2\beta_2^z - P_z^2 A) F_4^* \right]. \quad (A3)
\end{aligned}$$

---

[1] R. G. Sachs, Phys. Rev. **126**, 2256 (1962).

[2] M. Burkardt, Phys. Rev. D **62**, 071503 (2000) [erratum: Phys. Rev. D **66**, 119903 (2002)].

[3] M. Burkardt, Int. J. Mod. Phys. A **18**, 173 (2003).

- [4] A. V. Belitsky and A. V. Radyushkin, Phys. Rept. **418**, 1 (2005).
- [5] D. R. Yennie, M. M. Levy, and D. G. Ravenhall, Rev. Mod. Phys. **29**, 144 (1957).
- [6] G. A. Miller, Phys. Rev. Lett. **99**, 112001 (2007).
- [7] C. E. Carlson and M. Vanderhaeghen, Phys. Rev. Lett. **100**, 032004 (2008).
- [8] M. Strikman and C. Weiss, Phys. Rev. C **82**, 042201 (2010).
- [9] S. Venkat, J. Arrington, G. A. Miller and X. Zhan, Phys. Rev. C **83**, 015203 (2011).
- [10] U. Yakshiev and H.-Ch. Kim, Phys. Lett. B **726**, 375 (2013).
- [11] C. Granados and C. Weiss, JHEP **01**, 092 (2014).
- [12] D. Chakrabarti and C. Mondal, Eur. Phys. J. C **74**, 2962 (2014).
- [13] A. Silva, D. Urbano and H.-Ch. Kim, PTEP **2018**, 023D01 (2018).
- [14] J. H. Jung, U. Yakshiev and H.-Ch. Kim, Phys. Rev. D **93**, 054016 (2016).
- [15] C. Mondal, Phys. Rev. D **94**, 073001 (2016).
- [16] A. V. Gramolin and R. L. Russell, Phys. Rev. D **105**, 054004 (2022).
- [17] J. M. Alarcón and C. Weiss, Phys. Rev. D **106**, 054005 (2022).
- [18] J. Y. Panteleeva, E. Epelbaum, J. Gegelia and U. G. Meißner, Phys. Rev. D **106**, 056019 (2022).
- [19] C. Alexandrou, T. Korzec, G. Koutsou, C. Lorcé, J. W. Negele, V. Pascalutsa, A. Tsapalis and M. Vanderhaeghen, Nucl. Phys. A **825**, 115 (2009).
- [20] D. Chakrabarti and C. Mondal, Eur. Phys. J. A **52**, 285 (2016).
- [21] H. Alharazin, B. D. Sun, E. Epelbaum, J. Gegelia and U. G. Meißner, [arXiv:2212.11505 [hep-ph]].
- [22] C. E. Carlson and M. Vanderhaeghen, Eur. Phys. J. A **41**, 1 (2009).
- [23] C. Mondal, D. Chakrabarti and X. Zhao, Eur. Phys. J. A **53**, 106 (2017).
- [24] C. Huang and B. Q. Ma, Nucl. Phys. A **968**, 14 (2017).
- [25] C. Lorcé and P. Wang, Phys. Rev. D **105**, 096032 (2022).
- [26] G. A. Miller, Phys. Rev. C **79**, 055204 (2009).
- [27] M. V. Polyakov, JETP Lett. **90**, 228 (2009).
- [28] G. A. Miller, M. Strikman and C. Weiss, Phys. Rev. D **83**, 013006 (2011).
- [29] S. i. Nam and H.-Ch. Kim, Phys. Lett. B **707**, 546 (2012).
- [30] N. A. Mecholsky, J. Meija-Ott, M. Carmignotto, T. Horn, G. A. Miller and I. L. Pegg, Phys. Rev. C **96**, 065207 (2017).
- [31] N. Kumar, Phys. Rev. D **99**, 014039 (2019).
- [32] D. Fu, B. D. Sun and Y. Dong, Phys. Rev. D **105**, no.9, 096002 (2022).
- [33] E. Epelbaum, J. Gegelia, N. Lange, U. G. Meißner and M. V. Polyakov, Phys. Rev. Lett. **129**, no.1, 012001 (2022).
- [34] C. Alexandrou, C. N. Papanicolas and M. Vanderhaeghen, Rev. Mod. Phys. **84**, 1231 (2012).
- [35] C. Lorcé, Phys. Rev. Lett. **125**, 232002 (2020).
- [36] P. L. Chung, W. N. Polyzou, F. Coester and B. D. Keister, Phys. Rev. C **37**, 2000 (1988).
- [37] J. A. Rinehimer and G. A. Miller, Phys. Rev. C **80**, 025206 (2009).
- [38] J. Y. Kim and H.-Ch. Kim, Phys. Rev. D **104**, 074003 (2021).
- [39] Y. Chen and C. Lorcé, Phys. Rev. D **106**, 116024 (2022).
- [40] J. Y. Kim, Phys. Rev. D **106**, 014022 (2022).
- [41] S. Nozawa and D. B. Leinweber, Phys. Rev. D **42**, 3567 (1990).
- [42] V. Pascalutsa, M. Vanderhaeghen and S. N. Yang, Phys. Rept. **437**, 125 (2007).
- [43] J. Y. Kim and H.-Ch. Kim, Eur. Phys. J. C **79**, 570 (2019).
- [44] W. N. Polyzou, W. Glöckle and H. Witala, Few Body Syst. **54**, 1667 (2013).
- [45] C. Lorcé and P. Lowdon, Eur. Phys. J. C **80**, 207 (2020).
- [46] C. Lorcé, Eur. Phys. J. C **78**, 785 (2018).
- [47] C. Lorcé, H. Moutarde and A. P. Trawiński, Eur. Phys. J. C **79**, 89 (2019).
- [48] J. Y. Kim, B. D. Sun, D. Fu and H.-Ch. Kim, [arXiv:2208.01240 [hep-ph]].
- [49] R. L. Workman *et al.* [Particle Data Group], PTEP **2022**, 083C01 (2022).